NATIONAL & KAPODISTRIAN

UNIVERCITY OF ATHENS

MSC IN OCEANOGRAPHY AND MANAGEMENT
OF THE MARINE ENVIRONMENT

Response of the Arabian seas at the change of wind strength using a numerical model

Vasiliki Metheniti

(217014)

Supervised by

Sofianos Sarantis, Assist. Prof.

Athens, May 2019

Abstract

In this thesis, we consider an increase in wind speed over the wider region of Arabian seas, by conducting an experiment using a numerical ocean model (NEMO). The average annual response of the region was examined through the comparison between results of the experiment and the reference, as to different thermohaline and dynamical features, namely temperature, salinity and their surface values, sea surface height, latent heat flux and surface squared velocity. The region was divided into separate domains, selected by morphological and dynamical features. From basins of estuarine type (Red Sea, Arabian Gulf) and gulfs connecting them to the open ocean (Gulf of Aden, Gulf of Oman), to the Arabian Sea, we investigated the behavior of each basin of the Arabian seas, in order to conclude the possible driving mechanism(s) that seems to regulate their circulation. As a result, buoyancy fluxes seem to dominate in enclosed basins, while Ekman transport seems to be mainly responsible for the rest of the basins.

Key words: ocean numerical modelling NEMO, Arabian Seas, air-sea interaction

Περίληψη

Στη παρούσα διπλωματική εργασία, θεωρούμε μια αύξηση στην ταχύτητα του ανέμου, πάνω από την περιοχή των Αραβικών θαλασσών, με χρήση αριθμητικού μοντέλου (NEMO). Εξετάστηκε η μέση ετήσια απόκριση της περιοχής, μέσω της σύγκρισης των αποτελεσμάτων του πειράματος και της αναφοράς, ως προς τα διαφορετικά θερμοαλατικά και δυναμικά χαρακτηριστικά, ονομαστικά θερμοκρασία, αλατότητα και οι επιφανειακές τους τιμές, μέσο ύψος θάλασσας, λανθάνουσα ροή θερμότητας και τετράγωνο επιφανειακής ταχύτητας. Η περιοχή διαχωρίστηκε σε διαφορετικές υπολεκάνες, οι οποίες επιλέχθηκαν με βάση τα μορφολογικά και δυναμικά χαρακτηριστικά τους. Από ημίκλειστες λεκάνες (Ερυθρά θάλασσα, Αραβικός Κόλπος) και κόλπους που τις συνδέουν με τον ανοιχτό ωκεανό (Κόλπος του Άντεν, Κόλπος του Ομάν), στην Αραβική θάλασσα, προσεγγίσαμε τη συμπεριφορά κάθε λεκάνης των Αραβικών θαλασσών, με σκοπό να καταλήξουμε στο πιθανό μηχανισμό (ή μηχανισμούς) που φαίνονται να καθορίζουν την κυκλοφορία τους. Ως αποτέλεσμα, φαίνεται ότι οι ροές πλευστότητας κυριαρχούν στις ημίκλειστες λεκάνες, ενώ οι μεταφορές κατά Ekman φαίνονται να είναι υπεύθυνες για τις υπόλοιπες λεκάνες.

Λέξεις κλειδιά: ωκεανογραφικό αριθμητικό μοντέλο NEMO, Αραβικές θάλασσες, αλληλεπίδραση ατμόσφαιρας-θάλασσας

Acknowledgments

I would like to thank my supervisor Sarantis Sofianos, for the opportunity of working on such an interesting subject, and for his valuable contribution throughout the implementation of this thesis. I also want to thank Dr. Vasileios Vervatis for his helpful suggestions, as well as the rest of the laboratory. Last but not least, I would like to thank my fellow classmates and friends, and my family for their support.

List of Content

1. Introduction 8
1.1 Objectives 8
1.2 Red Sea 9
1.3 Gulf of Aden 11
1.4 Arabian Gulf 12
1.5 Gulf of Oman 13
1.6 Arabian Sea 14
2. Methodology 17
2.1 Model description 17
2.2 Inputs 18
2.2.1 Open Boundary Inputs 18
2.2.2 Atmospheric Inputs 19
2.2.3 Temperature/Salinity Inputs 19
2.2.4 River runoff inputs 19
2.3 The configuration 19
2.3.1 Reference 20
2.3.2 Experiment 20
2.4 Post processing analysis methods and tools 21
3. Results 23
3.1 General Response 23
3.2 Response per Domain 26
3.2.1 Response of Red Sea 26
3.2.2 Response of Arabian Gulf 34
3.2.3 Response of Gulf of Aden 41
3.2.4 Response of Gulf of Oman 48
3.2.5 Response of Arabian Sea 54
4. Conclusion 60
5. References 62

List of Figures

Figure 2-1: Bathymetry of the AMSG36 configuration. Point A denotes the Strait of Bab el Mandeb and point B the strait of Hormuz.....20
Figure 3-1: Full Domain- Spatial variability of the difference between the average annual values (Experiment-Reference) of Sea Surface Salinity (SSS), Sea Surface Temperature (SST), Sea Surface Height (SSH), Latent Heat Flux (Ql), for year 10 of the experiment.....25
Figure 3-2: Red Sea-Spatial variability of Sea Surface Salinity average annual values for year 10 of the experiment, the reference and their difference.....29
Figure 3-3: Red Sea- Spatial variability of Sea Surface Temperature average annual values for year 10 of the experiment, the reference and their difference. 30
Figure 3-4: Red Sea-Spatial variability of Latent Heat Flux average annual values for year 10 of the experiment, the reference and their difference.....31
Figure 3-5: Red Sea- Spatial variability of Sea Surface Height average annual values for the last year of the experiment, the reference and their difference. 32
Figure 3-6: Red Sea- Spatial variability of Sea Surface Squared Velocity average annual values for year 10 of the experiment, the reference and their difference. 33
Figure 3-7: Arabian Gulf- Spatial variability of Sea Surface Salinity average annual values for year 10 of the experiment, the reference and their difference. 36
Figure 3-8: Arabian Gulf- Spatial variability of Sea Surface Temperature average values for year 10 of the experiment, the reference and their difference. 37
Figure 3-9: Arabian Gulf- Spatial variability of average annual Latent Heat Flux for year 10 of the experiment, the reference and their difference.....38
Figure 3-10: Arabian Gulf- Spatial variability of Sea Surface Height average annual values for year 10 of the experiment, the reference and their difference. 39
Figure 3-11: Arabian Gulf- Spatial variability of Sea Surface Squared velocity average annual values for year 10 of the experiment, the reference and their difference. 40
Figure 3-12: Gulf of Aden- Spatial variability of Sea Surface Salinity average annual values for year 10 of the experiment, the reference and their difference. 43
Figure 3-13: Gulf of Aden - Spatial variability of Sea Surface Temperature average annual values for year 10 of the experiment, the reference and their difference. 44
Figure 3-14: Gulf of Aden- Spatial variability of average annual Latent Heat Flux for year 10 of the experiment, the reference and their difference.....45
Figure 3-15: Gulf of Aden - Spatial variability of Sea Surface Height average annual values for year 10 of the experiment, the reference and their difference. 46
Figure 3-16: Gulf of Aden - Spatial variability of Sea Surface Squared Velocity average annual values for year 10 of the experiment, the reference and their difference. 47
Figure 3-17: Gulf of Oman- Spatial variability of Sea Surface Salinity average annual values for year 10 of the experiment, the reference and their difference. 49
Figure 3-18: Gulf of Oman- Spatial variability of Sea Surface Temperature average annual values for year 10 of the experiment, the reference and their difference. 50
Figure 3-19: Gulf of Oman- Spatial variability of average annual Latent Heat Flux for year 10 of the experiment, the reference and their difference.....51
Figure 3-20: Gulf of Oman- Spatial variability of Sea Surface Height average annual values for year 10 of the experiment, the reference and their difference. 52
Figure 3-21: Gulf of Oman- Spatial variability of Sea Surface Squared Velocity average annual values for year 10 of the experiment, the reference and their difference. 53

Figure 3-22: Arabian Sea- Spatial variability of Sea Surface Salinity average annual values for year 10 of the experiment, the reference and their difference. 55
Figure 3-23: Arabian Sea- Spatial variability of Sea Surface Temperature average annual values for year 10 of the experiment, the reference and their difference. 56
Figure 3-24: Arabian Sea- Spatial variability of average annual Latent Heat Flux for year 10 of the experiment, the reference and their difference.....57
Figure 3-25: Arabian Sea- Spatial variability of Sea Surface Height average annual values for year 10 of the experiment, the reference and their difference. 58
Figure 3-26: Arabian Sea- Spatial variability of Sea Surface Squared Velocity average annual values for year 10 of the experiment, the reference and their difference. 59

List of Tables

Table 3-1: Full Domain-Average annual values of the results of the experiment and the reference, and their difference. 24
Table 3-2: Average annual values of the strength of the volume exchange at the strait of Bab el Mandeb. 27
Table 3-3: Red Sea- Average annual values of the results of the experiment and the reference, and their difference. 28
Table 3-4: Average annual values of the strength of the volume exchange at the strait of Hormuz. 35
Table 3-5: Arabian Gulf- Average annual values of the results of the experiment and the reference, and their difference. 35
Table 3-6: Gulf of Aden- Average annual values of the results of the experiment and the reference, and their difference. 42
Table 3-7: Gulf of Oman- Average annual values of the results of the experiment and the reference, and their difference. 48
Table 3-8: Arabian Sea- Average annual values of the results of the experiment and the reference, and their difference. 54

1. Introduction

1.1 Objectives

Wind stress on ocean surface is one of the most significant driving forces of its circulation, via friction (Ekman transport) on the surface layer, the convergence/divergence of which drive the interior ocean circulation. The other driving mechanism of circulation is buoyancy forcing, which is the sum of heat and freshwater air-sea fluxes (Evaporation minus Precipitation, E-P). The evaporation flux is directly related to latent heat flux, major terms of which are wind speed over the ocean surface and relative humidity. Latent heat flux is related to surface cooling and affects surface salinity, while it is responsible for regulating most of large-scale atmospheric circulation (through heat release). Furthermore, an indirect correlation between latent heat flux anomalies and wind speed strengthening have been found by Li et al. (2011).

The purpose of this thesis is the investigation on the effect of the strengthening of wind speed on the thermohaline and dynamical features of the Arabic seas. This region consists of basins of different morphological features, namely the Red Sea and the Arabian Gulf that are shallow semi enclosed seas connected with the Indian ocean through shallow straits, the Gulf of Oman and the Gulf of Aden which are connected with the Indian Ocean through wider mouths and the Arabian Sea the northwestern part of Indian Ocean.

A distinctive feature of this area is its relationship with the Indian monsoon system, as the seasonality of the winds greatly affect the circulation of the region. Monsoon is a seasonal phenomenon accompanied by wind reversal regimes, in which the temperature difference between the air above the sea and the land caused by solar radiation, creates a pressure gradient, as well as a shift of ITCZ. This pressure gradient draws moist air from above the ocean, over the land where it rises and condenses, resulting in rainfall. Summer or southwest

Monsoon (June-September), drives winds from the southwest toward the Indian landmass collecting moisture over the Arabian sea, resulting in great precipitation when they arrive over the land. Winter or northeast Monsoon (December-February), if less intense, with winds coming from northeast, causing less precipitation. Moreover, evaporation rates over Arabian seas are very high. So, due to this intense atmospheric forcing, through heat fluxes and wind stress, Arabic seas compose an ideal test case for the investigation of the upper ocean dynamics response. Here follows a brief description of the basin's main features.

1.2 Red Sea

The Red sea is a semi enclosed elongated basin, located between Africa and Asia continents, with a NW to SE orientation, starting at 12.5°N up until 30°N. It is connected on the northern part, to the Mediterranean Sea through the Suez Canal, which leads to the Gulf of Suez and the Gulf of Aqaba. On the southern part, a very narrow and shallow channel (160m depth, 25km wide narrowest point), the strait of Bab el Mandeb, connects the Red Sea with Gulf of Aden, and consequently with the Indian Ocean (Sofianos and Johns, 2007). Red Sea's average width is 220km, max length is 2250km while its mean depth is at 524m, with maximum values up to 3000m.

The Red Sea is enclosed by two desert areas, so the climate that prevails in the region is arid with very low precipitation rates, while river runoff is limited (often neglected) and heat loss has been estimated at $11\pm5 Wm^{-2}$ (Sofianos & Johns, 2002). Thus, all these factors in addition to an extensive evaporation rate and a freshwater flux estimated at 2.06±0.22 m/y (Sofianos, Johns, & Murray, 2002), result in high temperatures and the formation of one of the world's highest salinity water mass, the Red Sea Outflow Water (RSOW).

For the maintenance of the salinity budget, an exchange with the adjacent basins is taking place. The exchange through Suez Canal can be considered negligible (Sofianos and

Johns, 2015), so the main exchange is through the strait of Bab el Mandeb. The exchange is of inverse estuarine type, with a two-layer exchange during winter and a three-layer exchange during summer. Thus, there is an intrusion in the basin of low-salinity water from Gulf of Aden, while Red sea's high salinity water (RSOW) is released to the Indian ocean through Gulf of Aden as a deep outflow. The exchange is displaying strong seasonal variability, with maximum outflow estimated to be 0.6 Sv during winter and minimum at 0.05 Sv during summer (Murray and Johns, 1997; Bower, Hunt and Price, 2000). A characteristic of the exchange is that it flows over a very shallow sill, into a more stratified ocean. Moreover, the advection of the outflow water is been carried through narrow boundary currents in the Gulf of Aden and away from the sill (Bower, Hunt and Price, 2000), while traces of Red Sea water has been found into the equatorial and subtropical regions of the Indian Ocean (Beal, Ffield and Gordon, 2000).

The direction of the wind over the basin is influenced by two weather systems, and by the orography of the region. The high mountains along both sides of the basin influence the local dominant wind regimes, resulting in along-axis winds over Red Sea (Langodan *et al.*, 2016). North of 19° over basin, the winds are from north to northwest throughout the year, affected by the eastern Mediterranean weather systems, while south of 19° they are influenced by the Indian monsoon, so they reverse from south-southeast (during northeast monsoon) to northwest (during southwest monsoon).

Both buoyancy loss (mostly due to evaporation) and wind forcing, seem to play an important role in the circulation of the basin (Geyer and MacCready, 2014), but it is not certain how much each one contributes to the general patterns. The examination is mostly based on the exchange at the strait and its seasonality and while the most dominant theory is that thermohaline forcing regulates the circulation, others believe the wind forcing that is associated with the circulation's reversal, to be responsible instead (Patzert, 1974).

1.3 Gulf of Aden

Gulf of Aden is the receptor basin of RSOW, extending to eastward where it connects with the Arabian sea through a wider and deeper mouth. The gulf is enclosed by Yemen to the north and Somalia to the south.

Similar to Red Sea, the climate of the region is arid and the annual heat gain has been estimated at $113 Wm^{-2}$, and considering the area of the gulf ($220 \times 10^3 km$) the equivalent energy amount is remarkably high (Sultan and Ahmad, 1997).

The wind field is controlled by the reversing Indian monsoon and the circulation is formed of local cyclonic and anticyclonic eddies (Bower, Hunt and Price, 2000; Carton, L'hegaret and Baraille, 2012). During northeast monsoon, the winds over the east part of the gulf are from east turning to southeast closer to Bab el Mandeb, so that less saline water is penetrating into the Red Sea and water from the Arabian sea enters the gulf.

Respectively, during southwest monsoon, the prevailing winds over the gulf are from west-southwest over the western part and getting closer to Red Sea they become northwesterly. These winds induce extensive upwelling, especially during summer monsoon, where the winds are more intense, while another factor contributing to the upwelling in the western part is the convergence of the flow due to the exchange with Red Sea's water (Morcos and AbdAllah, 2012). Carton et al. (2012), after analysing argo float data, found that RSOW concentrates on the southwestern part of the gulf. Afterwards, mesoscale eddies develop in the basin and aid in the mixing and advection of RSOW, alternating its characteristics before it travels further into the Arabian sea as an intermediate water mass (Beal, Ffield and Gordon, 2000; Bower *et al.*, 2002; Carton, L'hegaret and Baraille, 2012). Thus, the heat gain mentioned above can be balanced through these mechanisms of upwelling and water exchange with the adjacent basins (Sultan and Ahmad, 1997).

1.4 Arabian Gulf

Arabian Gulf is a very shallow semi enclosed sea, surrounded by Iran and Iraq, on the northwest and northeast, and by Saudi Arabia on the southeast. It is elongated from northwest to southeast between latitudes of 24°-30°, with a length of 1000km, width of 338km and an average depth of 36m (Michael Reynolds, 1993). At the southern end the gulf gradually deepens throughout the strait of Hormuz (~56km wide) and into the Gulf of Oman and the Indian Ocean, so that there is no sill formation.

The winds over the gulf are dominantly northwesterlies (called Shamals) and they are greatly influenced by orography. However, getting closer to the strait of Hormuz they are influenced by the Indian monsoon r(Michael Reynolds, 1993; Pous, Carton and Lazure, 2013).

The gulf is exposed to arid, subtropical climate, as it is contiguous to the desert of Saudi Arabia, and an excessive evaporation rate, which is driven by high wind speeds. Observations derived by Johns et al. (2003) estimate the net evaporation over the basin to be at 1.68±0.39 m/y. The annual net surface heat loss over the gulf has been estimated at -6W/m^2, with greatest heat loss in southeastern and northwestern regions of the Gulf, while there is large spatial variation in latent heat flux (Rezaei-Latifi and Hosseinibalam, 2015).

The circulation in the basin is of inverse estuary type, driven mainly by buoyancy losses (due to evaporation). Indeed, in order to balance this loss, an exchange is taking place at the strait of Hormuz, where a surface inflow of less saline water from the Indian Ocean enters the gulf (Indian Ocean Surface Water, IOSW) and a dense, hypersaline water mass exits from bellow, as there is no sill to constrain it (Johns *et al.*, 2003).

According to model results by Yao and Johns, (2010), after the IOSW enters the gulf, it separates into two branches. One branch is travelling to the north along the coast of Iran (with the more intense intrusion during summer) and the other is spreading to the southern basin by

Ekman drifting, due to winds- both forming cyclonic features on the corresponding parts of the basin. The densest waters are forming on the northern part of the basin, and after losing buoyancy they ultimately exit through the strait as a deep flow, comprising a hypersaline water mass, one of the most saline water masses in the world ocean, the Persian Gulf Water (PGW) with a temperature of 22°C and salinity at 40 at the strait (Michael Reynolds, 1993; Johns *et al.*, 2003; Swift and Bower, 2003; Carton, L'hegaret and Baraille, 2012). Eventually, cascading down the continental slope, the outflow is forming a slope current near the Omani coast (Pous, Carton and Lazure, 2004). Furthermore, upwelling features have been observed along the Iranian coast (Pous, Carton and Lazure, 2004; Carton, L'hegaret and Baraille, 2012).

1.5 Gulf of Oman

The Gulf of Oman is located at 22°N-26° N, 56° E-60° E, surrounded by the Iranian and Oman coasts, opening to the Arabian Sea on its southeastern part. The Gulf of Oman can be characterized as a transition from the estuarine type circulation of the Arabian Gulf, to deep-ocean circulation (Michael Reynolds, 1993).

The prevailing winds follow the Indian monsoons seasonality, along northeast and southwest axis (from winter to summer monsoon) (Pous, Carton and Lazure, 2004). Close to the strait, PGW is mixed with IOSW, reducing its salinity (Pous, Carton and Lazure, 2004). During summer PGW has been found to escape the Gulf of Oman southeastward and into Arabian Sea (Carton, L'hegaret and Baraille, 2012). Moreover, gyre formations have been observed with anti-cyclonic encompassing cold water and induce upwelling features along the Iranian coast (Michael Reynolds, 1993; Pous, Carton and Lazure, 2004; Carton, L'hegaret and Baraille, 2012).

An annual mean heat loss at the sea surface has been documented, which is counterbalanced by heat flow through the strait of Hormuz (Sultan and Ahmad, 1993). During

winter the heat loss is compensated by heat advection from the Arabian Sea through currents, while in summer the heat gain is balanced by upwelling off the coast of Arabia.

1.6 Arabian Sea

The Arabian Sea is located at the northwestern part of the Indian Ocean and plays a critical role in the onset and evolution of the Indian monsoon, as well as in the associated precipitation over the Indian subcontinent (Centurioni *et al.*, 2017).

Arabian Sea is strongly depending on the Indian monsoon winds, as their seasonal reversal yields large changes in the oceans near-surface currents, as well as in its thermohaline features (Fischer *et al.*, 2002; Vecchi *et al.*, 2004). Another factor influencing the basin is air-sea heat fluxes, as the evaporation is very high, and the E-P budget is estimated to be around 1.50m/y (Carton, L'hegaret and Baraille, 2012). The water masses found in the basin, besides RSOW and PGW, are the Indian Central Water (ICW) with a vertical temperature range of 17°C to 5°C and salinity range between 35.5 and 34.8, the Indian Deep Water (IDW) that lies below ICW and has a potential temperature of 2.5°C and salinity at 34.8 and the Antarctic Bottom Water below 3800m (0.3°C, 34.7).

The monsoon wind cycle results in the annual reversal of a large boundary current, the Somali current, making it the only region in the world where that happens (Schott, 1983). The Somali current is located along the northeastern part of Africa, that flows northward during boreal summer, along the coast of Somalia, with surface currents exceeding 200cm/s, and southward during winter (Vecchi *et al.*, 2004; Schott, Xie and McCreary, 2009; Wang *et al.*, 2018). These currents form great eddy structures with the most notorious being the Great Whirl, an anticyclonic eddy off the Horn of Africa ranging between latitudes of 5°N -9°N, generated by baroclinic Rossby waves during southwest monsoon. Associated to these are distinguishing

SST features, with cold upwelled waters surrounded by warmer water (Schott *et al.*, 1982, 1997; Vecchi *et al.*, 2004).

During northeast monsoon, the wind forcing is mild to moderate and the heat budget is negative, and surface cooling has been found to intensify with offshore distance (Lee *et al.*, 2000), yielding in destabilized surface buoyancy flux. Moreover, the circulation of the Arabian sea is supplied by a westward propagation of the Northeast Monsoon Current (also known as North Equatorial Current) with a northwest Ekman transport (Schott and Fischer, 2000). This current carries water from the Bay of Bengal into the Arabian Sea, with part of it continuing into Gulf of Aden and another fraction travelling northern.

During southwest monsoon, strong wind forcing results in southeastward Ekman transpot and in neutral to strong stabilizing of surface and buoyancy fluxes (Fischer *et al.*, 2002). Along the southern coast of Oman, upwelled water is exported off the coast and into the Arabian sea forming cold jets, especially on the surface, reaching hundreds of kilometers into the interior (Lee *et al.*, 2000; Fischer *et al.*, 2002; Carton, L'hegaret and Baraille, 2012). Additionally, the Great Whirl is often formed during that period and Somali current communicates with Gulf of Aden mostly through the passages between Socotra and the African continent (Schott *et al.*, 1997). Furthermore, during southwest monsoon upper ocean heat loss has been observed which is balanced by a positive heat flux from the atmosphere, a negative northward heat flux and heat loss due to upwelling. Both seasons are accompanied by the cooling of the subsurface mixed layer of the ocean (Schott and Fischer, 2000).

Overall, the upper ocean heat budget and consequently SST values have been found to be influenced by solar heating, surface heat losses, turbulent & convective entrainment and horizontal heat advection, as well as vertical advection due to Ekman pumping (or the

associated mesoscale flows) (Düing *et al.*, 1980; Lee *et al.*, 2000; Fischer *et al.*, 2002, Roberts *et al.* 2017).

2. Methodology

2.1 Model description

The model used for the implementation of this thesis, is a global configuration built from the oceanic component of the Nucleus for European Modelling of the Ocean, NEMO. This modelling framework consists of ocean related engines studying the ocean, as well as its interaction with other components of earth's climate system, such us atmosphere, sea-ice, tracers etc, working over wide time and space scales. These engines are, namely, OPA1 for the ocean dynamics and thermodynamics, LIM2 for the sea-ice dynamics and thermodynamics, TOP3 for the biogeochemistry (both transport (TRP) and sources minus sinks (LOBSTER, PISCES) (Madec *et al.*, 1998; Madec, 2016). The model solves the 3-Dimentional primitive equations along with a nonlinear equation of state which couples the two active tracers (temperature and salinity) to the fluid velocity, in Arakawa C-grid. Furthermore, it considers the fluid to be incompressible and hydrostatic, it assumes spherical earth and thin shell approximation, as well as the Boussinesq and the turbulence closure hypothesis. Using an orthogonal set of unit vector (***i,j,k***) liked to the earth, we are working on the following equations:

Momentum Balance:

$$\frac{\partial \mathbf{U}_h}{\partial t} = [(\bigtriangledown \times \mathbf{U}) \times \mathbf{U}) + \frac{1}{2} \bigtriangledown (\mathbf{U}^2)]_h - f\mathbf{k} \times \mathbf{U}_h - \frac{1}{\rho_o} \bigtriangledown_h p + \mathbf{D}^{\mathbf{U}} + \mathbf{F}^{\mathbf{U}}$$

Hydrostatic equilibrium:

$$\frac{\partial p}{\partial z} = -\rho g$$

Incompressibility equation:

$$\bigtriangledown \cdot \mathbf{U} = 0$$

Heat conservation equation:

$$\frac{\partial T}{\partial t} = - \bigtriangledown \cdot (T\mathbf{U}) + D^T + F^T$$

Salt conservation equation:

$$\frac{\partial S}{\partial t} = - \bigtriangledown \cdot (S\mathbf{U}) + D^S + F^S$$

Equation of state:

$$\rho = \rho(T, S, p)$$

Where $\boldsymbol{U} = \boldsymbol{U}_k + w\boldsymbol{k}$, is the vector velocity (*h* denotes the horizontal plane), T is the potential temperature, S is the salinity, ρ the in-situ density, ρ_o is a reference density, p the pressure, $\mathrm{f} = 2\Omega\mathrm{k}$ is the Coriolis acceleration (where Ω is Earth's angular velocity vector), and g is the gravitational acceleration. D^u, D^T and D^S are the parameterisations of small-scale physics for momentum, temperature and salinity, and F^U, F^T and F^S surface forcing terms.

The ocean mesh (i.e. the position of all the scalar and vector points) is defined by the transformation that gives (λ, ϕ, z) geographical coordinate system as a function of orthogonal curvilinear coordinates (i, j, k), where λ(i,j) is the latitude coordinate and φ(i,j) the longitude coordinate.

2.2 Inputs

Below we mention the models inputs that were used for the conduction of the experiment. Tidal forcing was not considered.

2.2.1 Open Boundary Inputs

The South and East open boundary data for meridional and zonal velocity, sea surface height, salinity and temperature were created using ORCAs configurations data (Madec, 2016).

2.2.2 Atmospheric Inputs

As forcing inputs, the model uses the DRAKKAR Forcing Sets (DFS) (Dussin Raphael, Barnier Bernard, Brodeau Laurent, 2016), which have been developed using atmospheric reanalysis carried out at the European Centre for Medium Range Weather Forecast (ECMWF). In particular, the dataset used is DFS5.2, includes ERA-interim (ERAi) reanalysis data for the period 1979-2015. The variables of DFS5.2, required by NEMO bulk formula for calculations, are the zonal and meridional components of the 10-m wind (u10, v10), 2-m air humidity (q2), 2-m air-temperature (t2), downward shortwave radiation at the sea surface (radsw), downward longwave radiation at the sea surface (radlw) and precipitation. All fields are provided on a 0.7° grid, every 3h for u10, v10, q2, t2 and daily for radiation and precipitation.

2.2.3 Temperature/Salinity Inputs

The initialisation of ocean temperature and salinity was conducted using input data from the World Ocean Atlas, WOA set of climatological mean gridded fields (or else Levitus Climatology).

2.2.4 River runoff inputs

The river runoff is added to the surface box only and gives information about the salt content of it.

2.3 The configuration

For this experiment, we focused on the domain that constrains the Arabian sea, the Red Sea and the Arabian Gulf, for latitude values between 5.0-30.4 degrees and longitude between 32.2-70.9 degrees. The horizontal resolution of the configuration is 1/36° (approximately 3km) using a mesh of 1396x988 grids, making use of the ORCA tripolar grid. Bathymetry was provided by GEBCO data. The vertical grid consists of 50 levels of different size, while their

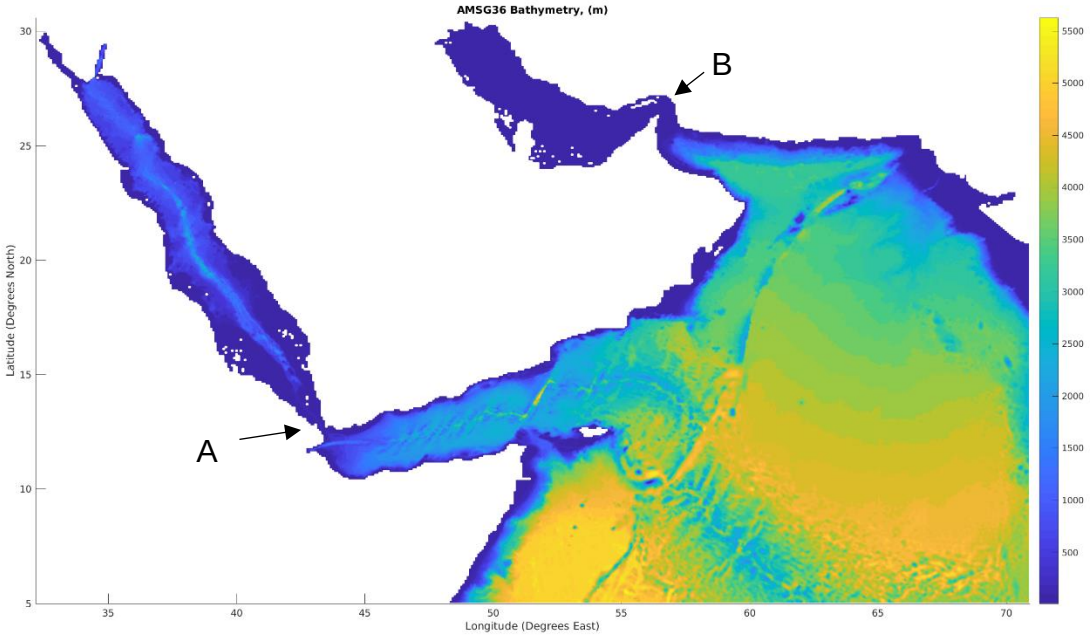

Figure 2-1: Bathymetry of the AMSG36 configuration. Point A denotes the Strait of Bab el Mandeb and point B the strait of Hormuz

size is increasing with depth from 1m to approximately 400m at the bottom. Additionally, there was no use of tidal parameters. From now on, this configuration will be referred to as AMSG36 (Figure 2-1). The model gives monthly outputs for the thermohaline features, velocities and downward heat fluxes.

.

2.3.1 Reference

The model had extracted outputs for 80 years during spin-up and hereinafter they will be referred to as reference data. For the purposes of this experiment, the final ten years of reference data were given.

2.3.2 Experiment

Objective of the experiment was to examine the general response of the AMSG36 domain's thermohaline and dynamical features, to the change in wind speed (and consequently wind stress, turbulent fluxes, evaporation etc.). To do so, we increased the wind speed variable,

u10 (as wind stress is a function of the dimensionless drag coefficient C_d and of the square of wind speed 10m above sea surface, $tau = \rho_{air} C_d U_{10}^2$). To determine an optimum value that would be multiplied to the existing wind speed field, the DFS5.2 zonal and meridional 10-m wind components, corresponding to the Indian monsoon index U850 region (40E-80E,5N-15N) (Wang *et al.* 1999), were processed. This area was selected due to the effect of the monsoonal winds over our area of interest. We obtained the summer mean field value of velocity for each year from the DFS5.2 extended dataset (years 1958-2015). The mean field value for U850 region for the years 1958-2015, was ~8.18m/s with a standard deviation of ±0.25m/s. After consideration we concluded that an increase by a factor of 1.05 was logical, as it is below the maximum summer mean value obtained (8.74 m/s, year 2013).

On the next step, we ran the model using the output of the 70th year of the reference run as a restarting file, and the multiplied by 1.05 u10, v10 DFS5.2 data as input. After obtaining monthly outputs (experiment data) for the next 10 years, and mean surface kinetic energy was stabilized, a comparison was held between the data of experiment and the reference, for the final year (hereinafter year 10).

2.4 Post processing analysis methods and tools

The means used for the process of the model's results where cdf tools, cdo tools, nco tools and matlab. The models output data that were used for the experiment were temperature and salinity and their surface values, sea surface height, latent heat flux, wind stress and the surface squared velocity and surface vorticity that were calculated using the ocean surface velocity components. Additionally, using surface velocities we estimated the water volume exchange of the Red Sea and the Arabian Gulf with the Indian Ocean, at the strait of Bab el Mandeb and at the strait of Hormuz respectively (Figure 2-1).

Tables listed on section 3, demonstrate the differences between average annual values the final year of the experiment and the reference. These values refer to temperature (T), salinity (S) and their corresponding surface features (SST, SSS), sea surface height (SSH), surface squared velocity (SU^2), surface vorticity (Sζ), latent heat flux (Qlat) and wind stress (tau). The positive sign of Qlat on the map, indicates the upward flux (energy leaving the ocean). Positive values of Qlat mean that the flux has been increased, hence if we consider that the evaporation rate is depending on that flux, positive value of Qlat results in enhanced evaporation rate. Hereinafter, all given values discussed in the text, correspond to the difference between the experiment and the reference (experiment value-reference value), unless it is stated otherwise. Along with the Tables, come maps of spatial variability of the average annual values for the experiment, the reference and their difference.

Using these results, an explanation of the general response of the domain was attempted. Afterwards, we separated the region into specified domains to get a closer look into the spatial variability of their features and consequently, to examine their response to the changes mentioned above.

3. Results

3.1 General Response

As a general response of the AMSG36 region to the intensification of wind speed, wind stress has increased. Additionally, both temperature and salinity, as well as their surface features have decreased, with surface values showing greater variability and SST being O(10) greater that T (Table 3-1,). Wind stress depends on wind speed and the drag coefficient (which in turns depends on surface temperature) as mentioned in 2.3.2. So, the increase of wind stress, even though SST value has decreased, denotes that wind speed is more important.

This results for temperature and salinity, could be due to excessive upwelling at the region and advection induced by the increased wind speed, which could explain the further decrease of surface values. Other factors contributing to the reduction of temperature are air-sea heat fluxes, which are affected by the wind field, and heat fluxes with the adjacent ocean induced by density driven currents related to evaporation. As Table 3-1 shows, latent heat flux has increased meaning the ocean is releasing more heat through evaporation, which could lead to buoyancy losses and cooling of the surface. Moreover, the surface kinetic energy of the domain increased (considering the mean kinetic energy as a function of the squared surface velocity) and the surface circulation seems to be more anticyclonic (negative surface vorticity difference, Table 3-1). Spatial variation of Sea Surface Height (SSH) is less prominent in Arabian Gulf, in relation to the other basins (Figure 3-1).

Full Domain	Experiment	Reference	Difference (Exp-Ref)
Tau(N/m^2)	0.077	0.069	0.008
Qlat(W/m^2)	134.8192	134.0985	0.721
$SU^2(m^2s^{-2})$	0.100	0.090	0.010
T(°C)	10.8529	10.8675	-0.015
SST(°C)	27.3487	27.4572	-0.109
S	35.8189	35.8326	-0.014
SSS	36.5397	36.5748	-0.035
SSH	0.2663	0.2689	-0.0026
$S\zeta$ (s^{-1})	-3.75e-08	-8.40e-8	-3.560e-09

Table 3-1: Full Domain-Average annual values of the results of the experiment and the reference, and their difference.

However, the response of individual regions within the domain varies. Below, we demonstrate the main features of the experiments results, for different domains that where selected according to their different geomorphological and dynamical attributes and the main forces that seem to regulate their flow.

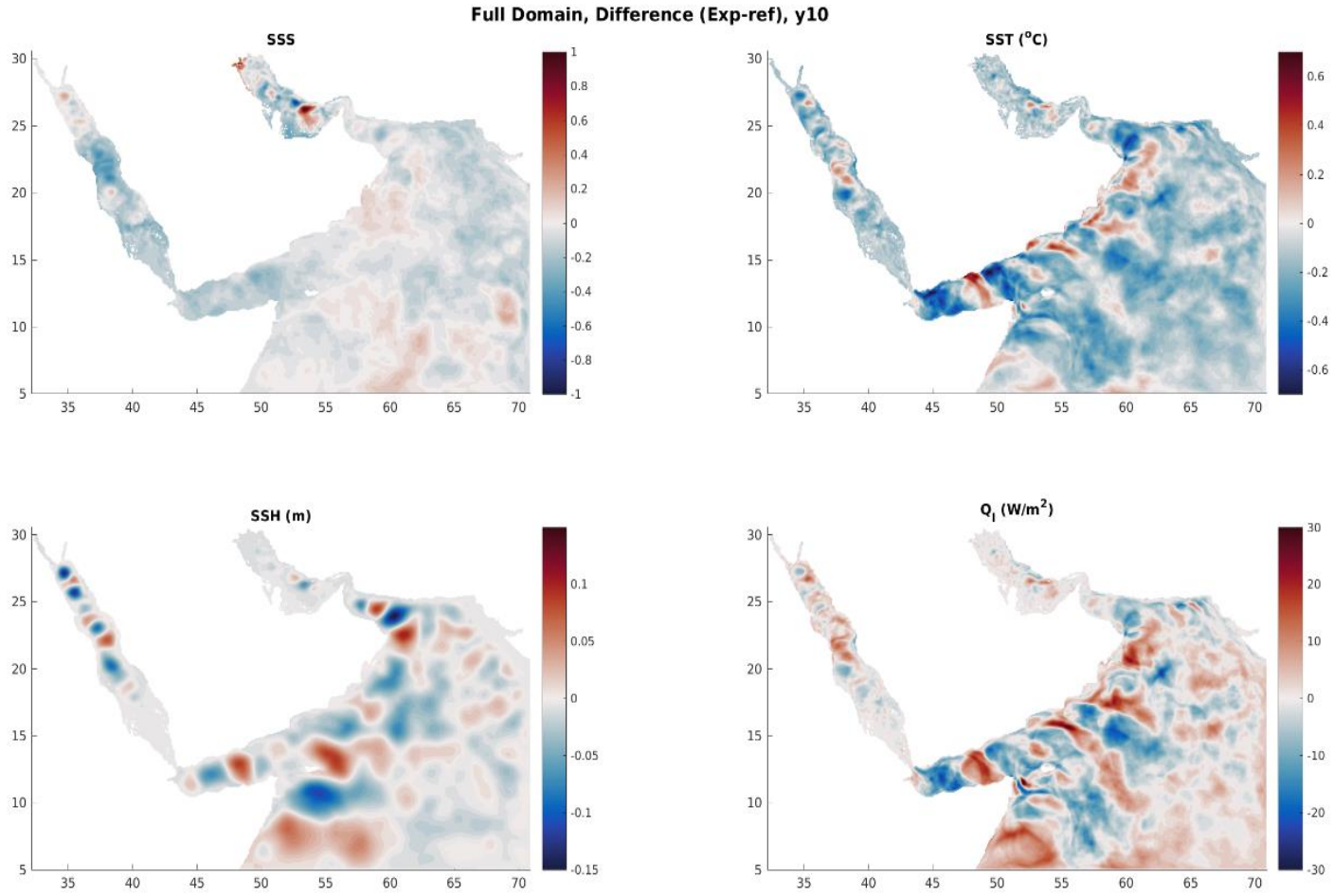

Figure 3-1: Full Domain- Spatial variability of the difference between the average annual values (Experiment-Reference) of Sea Surface Salinity (SSS), Sea Surface Temperature (SST), Sea Surface Height (SSH), Latent Heat Flux (Ql), for year 10 of the experiment

3.2 Response per Domain

The region was separated into five domains, that developed different response to atmospheric forcing by expressing different thermohaline and dynamical characteristics. These are: The Red Sea (RS), the Arabian Gulf (AG), the Gulf of Aden (GoA), the Gulf of Oman (GOM) and the Arabian Sea (AS). We examined the features that were listed above, as well as the main exchange between the RS and the AG with the adjacent gulfs, at the strait of Bab el Mandeb and the strait of Hormuz respectively.

3.2.1 Response of Red Sea

As mentioned in the Introduction, the exchange through Suez Canal is considered negligible, so the volumetric exchange between the RS and the GoA, was examined at the strait of Bab el Mandeb (BeM) (Figure 2-1). According to the results, the outflow exceeds the inflow, which could be due to the fact that the averaging included monthly inflow sometimes close to zero. In this case we are interested in the difference between the two experiments, so, we demonstrate the strength of the exchange and not the inflow and outflow values. Results show an increase in the strength of the exchange (Table 3-2). It is known that the dynamics of an enclosed sea, like Red Sea, are demonstrated at the strait that connects them with the open ocean (Cessi *et al.*, 2014). So, the results at BeM, indicate an enhanced overturning circulation.

Furthermore, salinity and temperature are reduced, while surface values appear to be more affected (Table 3-3). Latent heat flux has increased (Table 3-3,Figure 3-4) leading to higher evaporation rates. This higher latent heat flux seems to increase SSS and reduce SST on the northern part of the basin (Figure 3-2,Figure 3-3). As a result, it could be possible that

this area demonstrates an increase in the buoyancy flux, enhancing the pressure gradient, and correspondingly the exchange at the strait.

Additionally, the increased wind speed, resulting in increased wind stress, could induce the flow from the Gulf of Aden further up into the Red Sea. So less saline water is spreading up into the basin, lowering the surface salinity of that region, as well the total salinity of RS (Figure 3-2, Figure 3-3).

Moreover, as it was expected the wind stress increases, while the mean kinetic energy of the surface decreases (Table 3-3), and concentrates northern up the basin as it is illustrated in Figure 3-5 and Figure 3-6 of the sea surface height and surface squared velocity field. Another factor under consideration is the surface vorticity, which seems to decrease, making the circulation more anticyclonic.

Considering the results for surface mean kinetic energy and for the exchange at the strait, it is possible that the circulation of RS is mainly density driven, through the buoyancy losses caused by evaporation.

BeM	Experiment (Sv)	Reference (Sv)	Difference (Exp-Ref)(Sv)
Strength of the Exchange	0.593	0.584	0.01

Table 3-2: Average annual values of the strength of the volume exchange at the strait of Bab el Mandeb.

RS	Experiment	Reference	Difference (Exp-Ref)
Tau (N/m^2)	0.027	0.025	0.002
Qlat (W/m^2)	143.702	142.407	1.295
$SU^2(m^2s^{-2})$	0.034	0.039	-0.005
T(°C)	24.802	24.882	-0.080
SST(°C)	28.684	28.790	-0.106
S	38.872	38.918	-0.046
SSS	38.025	38.142	-0.117
SSH (m)	0.138	0.145	-0.007
$S\zeta$ (s^{-1})	-1.170e-07	-1.090e-07	-7.290e-09

Table 3-3: Red Sea- Average annual values of the results of the experiment and the reference, and their difference.

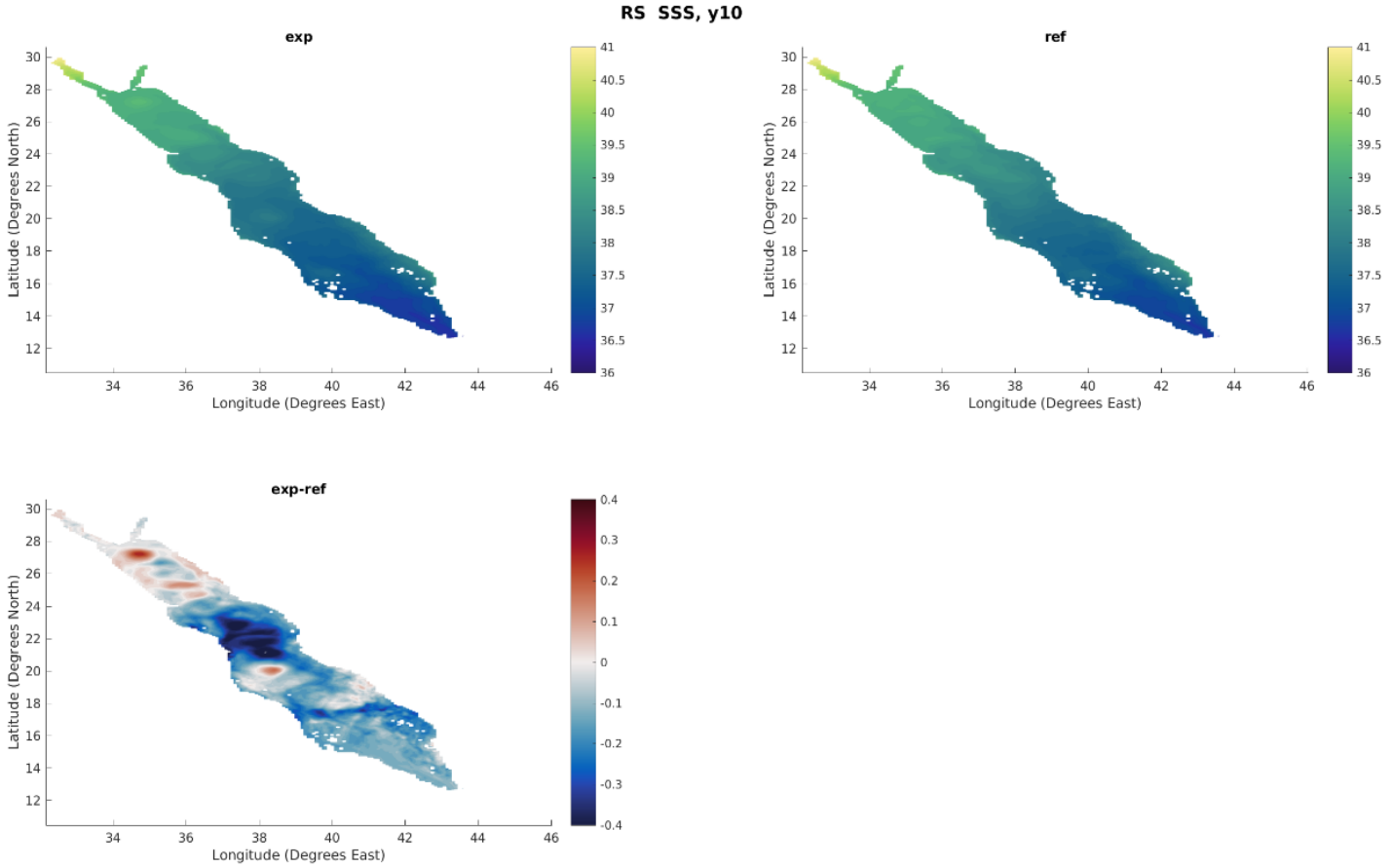

Figure 3-2: Red Sea-Spatial variability of Sea Surface Salinity average annual values for year 10 of the experiment, the reference and their difference.

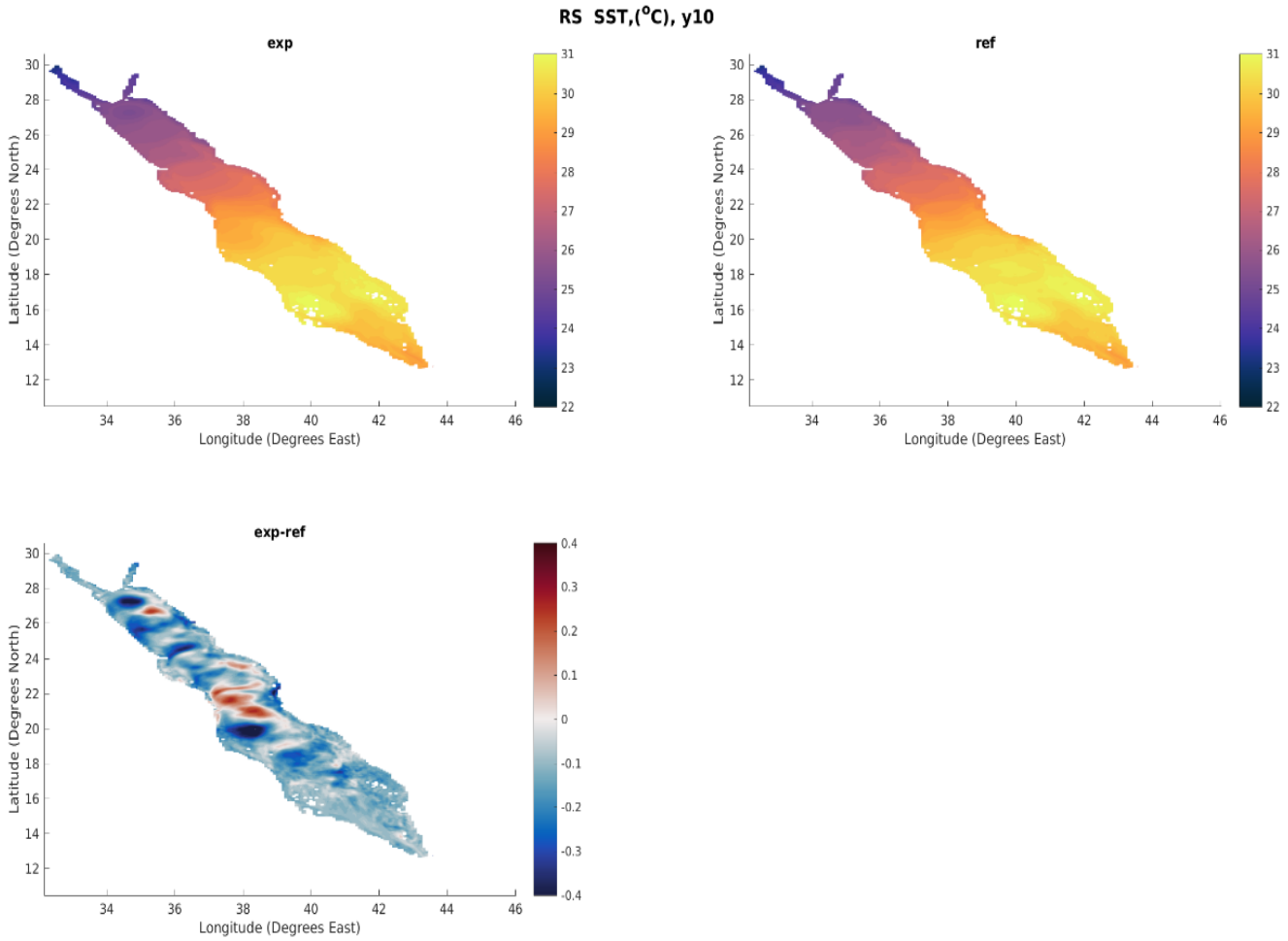

Figure 3-3: Red Sea- Spatial variability of Sea Surface Temperature average annual values for year 10 of the experiment, the reference and their difference.

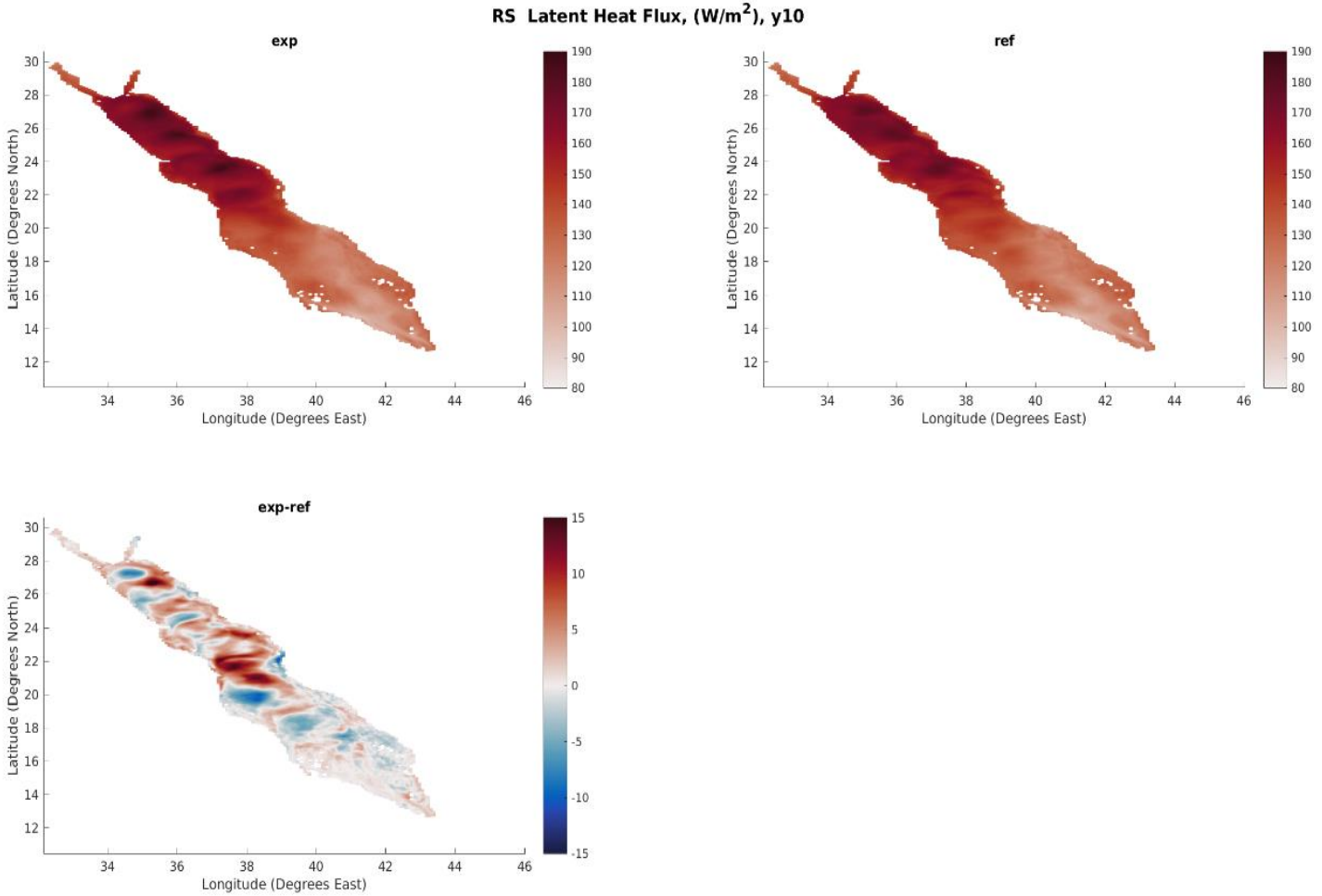

Figure 3-4: Red Sea-Spatial variability of Latent Heat Flux average annual values for year 10 of the experiment, the reference and their difference.

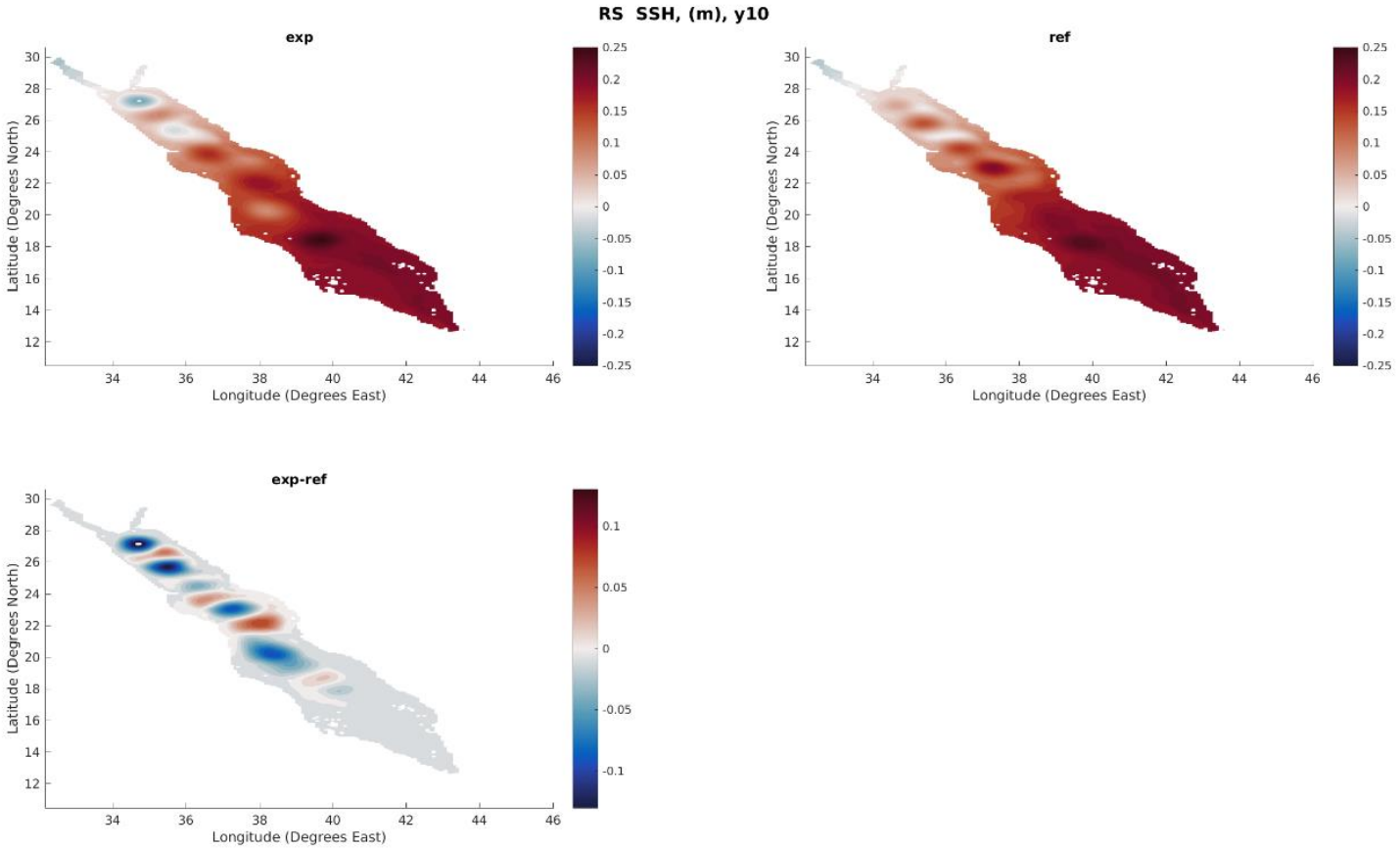

Figure 3-5: Red Sea- Spatial variability of Sea Surface Height average annual values for the last year of the experiment, the reference and their difference.

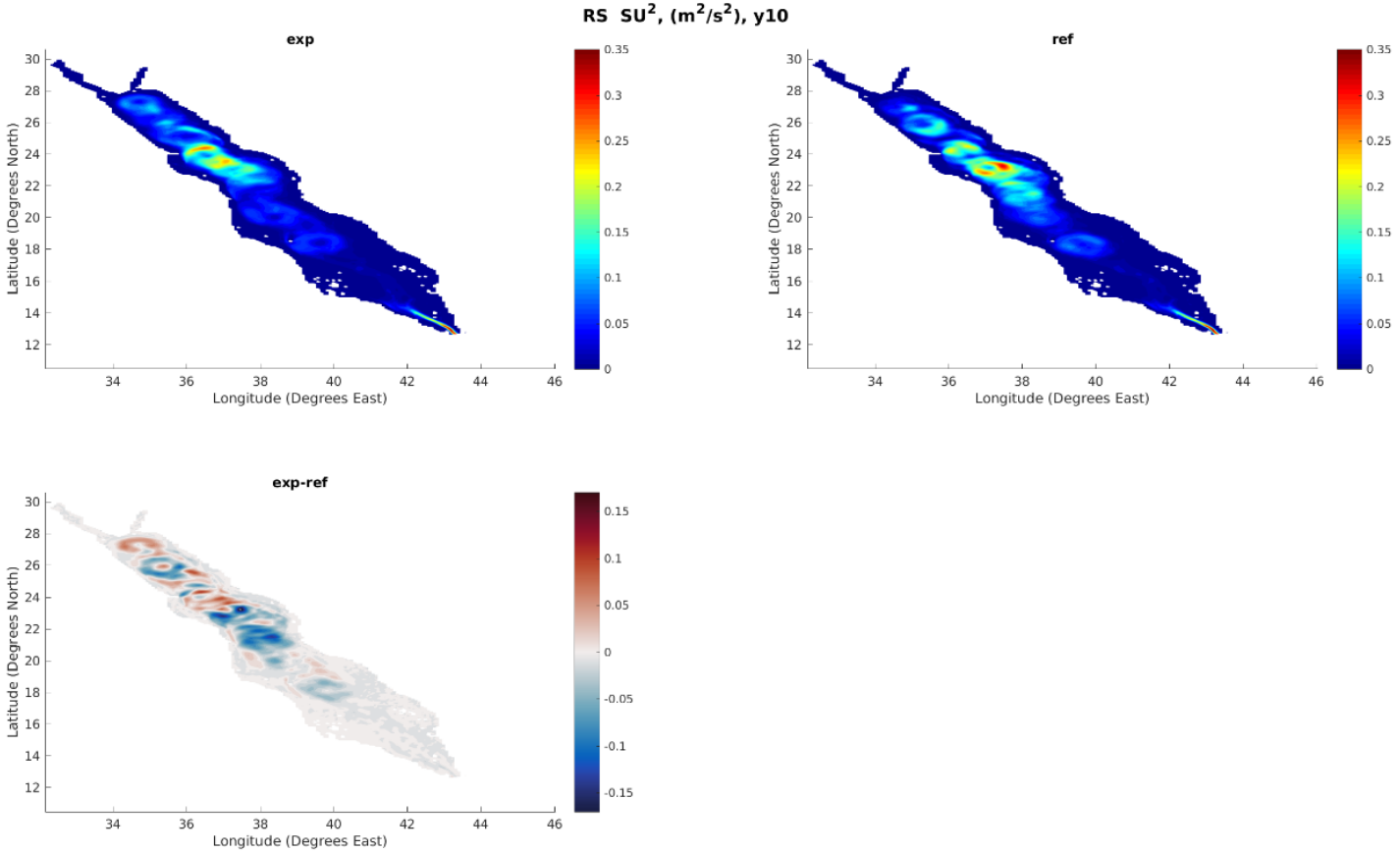

Figure 3-6: Red Sea- Spatial variability of Sea Surface Squared Velocity average annual values for year 10 of the experiment, the reference and their difference.

3.2.2 Response of Arabian Gulf

Similarly to RS, AG demonstrates an increase in its water volume exchange with the Indian Ocean, at the strait of Hormuz (Table 3-4). This transport demonstrates greater variability, in comparison with RS (Table 3-2). This may be due to excessive evaporation (as seen through latent heat flux, Table 3-5, Figure 3-9), leading to further buoyancy loss. The enhanced evaporation is also coherent with surface temperature values (Figure 3-8), as well as surface salinity values on the northern part of the gulf (Figure 3-7). However, surface salinity and the salinity of the whole gulf are reduced, which may be due to the enhanced exchange at the strait, as more fresh water from the Indian Ocean is entering the basin. Additionally, surface salinity shows greater spatial variability but lower average SSS value with respect to the Red Sea, probably due to enhanced local effects.

Furthermore, due to the positive vorticity difference (Table 3-5: Arabian Gulf-), it appears that the circulation is more cyclonic, leading the intruding water further up in the gulf as it can be seen in surface salinity and temperature maps (Figure 3-7, Figure 3-8). Additionally, looking at the SST maps (Figure 3-3) it seems that the upwelling along the coast of Iran is also enhanced, as the temperature has dropped. Moreover, the surface kinetic energy of the basin has decreased (portrayed by the surface squared velocity, Table 3-5,Figure 3-11), which can be compensated by the observed enhanced overturning circulation.

So, once again buoyancy loss seems to dominate over wind forcing, thus having the leading role for the circulation in the gulf. This comes in agreement with observations and studies conducted, as mention in Introduction.

Hormuz	Experiment (Sv)	Reference (Sv)	Difference (Exp-Ref)(Sv)
Strength of the Exchange	0.475	0.409	0.021

Table 3-4: Average annual values of the strength of the volume exchange at the strait of Hormuz.

AG	Experiment	Reference	Difference (Exp-Ref)
Tau (N/m^2)	0.016	0.015	0.001
Qlat (W/m^2)	119.553	118.593	0.960
SU^2 (m^2s^{-2})	0.0064	0.0066	-0.0002
T (°C)	26.157	26.224	-0.067
SST (°C)	27.447	27.535	-0.088
S	36.604	36.652	-0.048
SSS	39.153	39.201	-0.048
SSH (m)	0.140	0.145	-0.005
Sζ (s^{-1})	5.600e-08	3.730e-08	1.870e-08

Table 3-5: Arabian Gulf- Average annual values of the results of the experiment and the reference, and their difference.

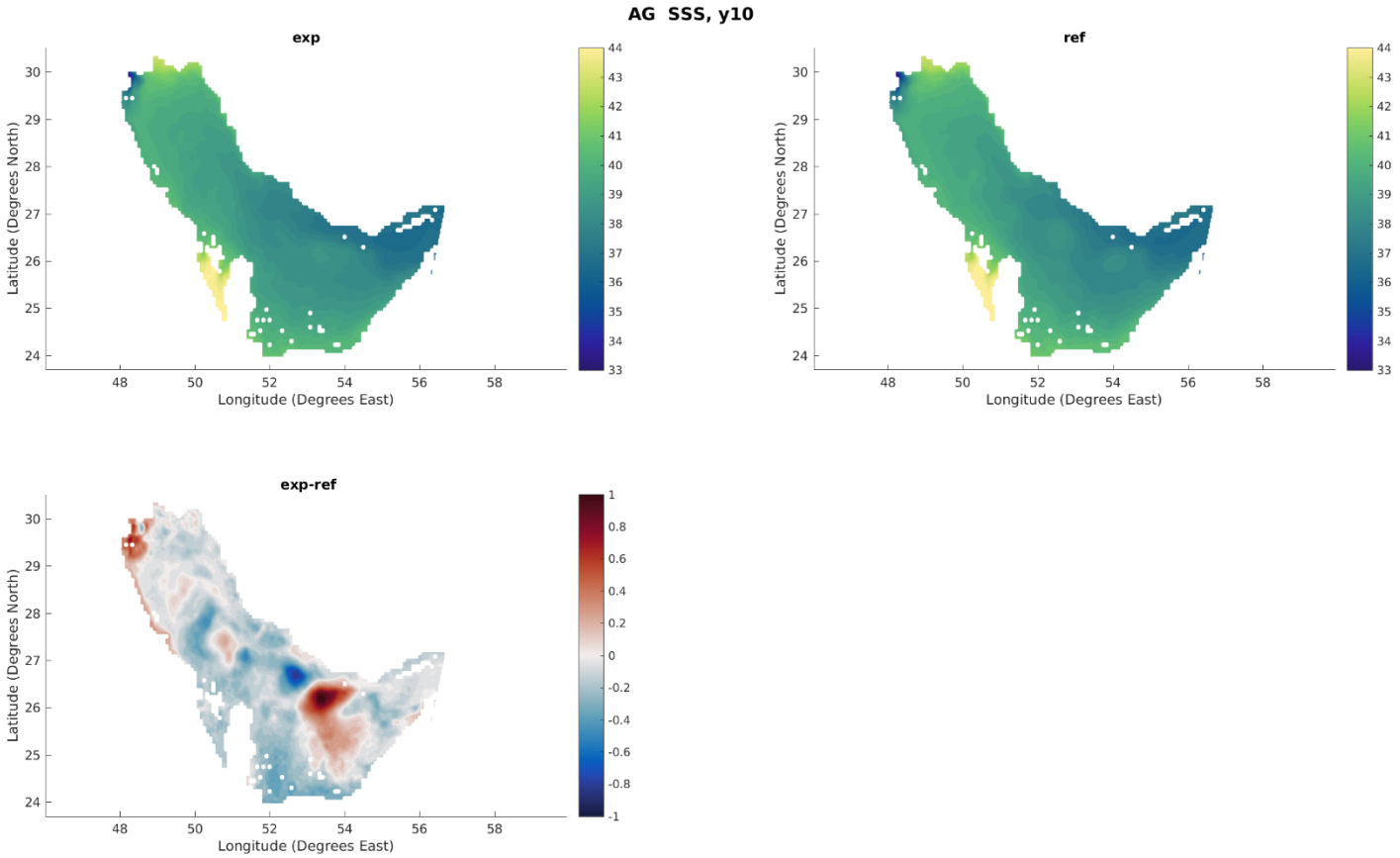

Figure 3-7: Arabian Gulf- Spatial variability of Sea Surface Salinity average annual values for year 10 of the experiment, the reference and their difference.

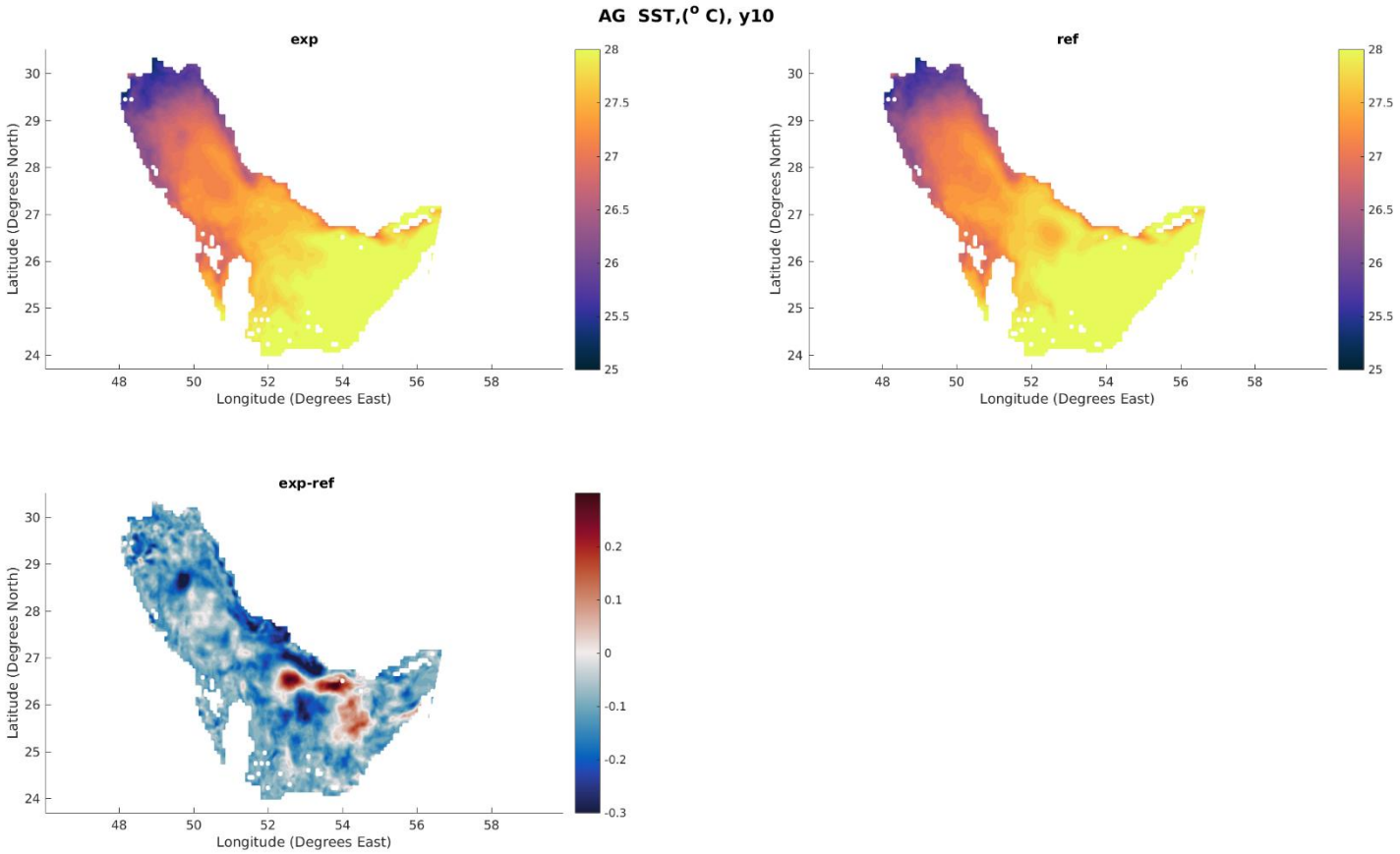

Figure 3-8: Arabian Gulf- Spatial variability of Sea Surface Temperature average values for year 10 of the experiment, the reference and their difference.

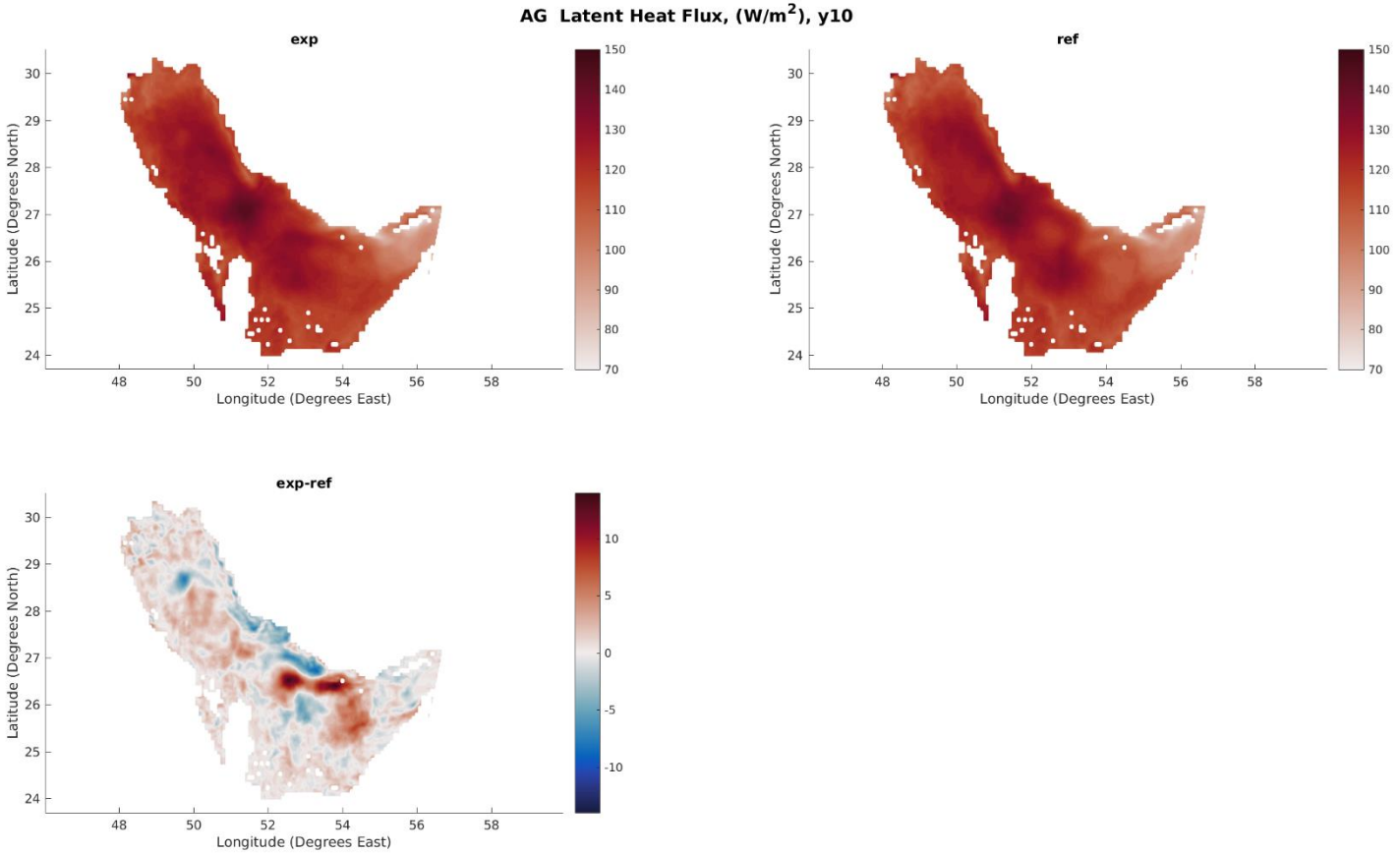

Figure 3-9: Arabian Gulf- Spatial variability of average annual Latent Heat Flux for year 10 of the experiment, the reference and their difference.

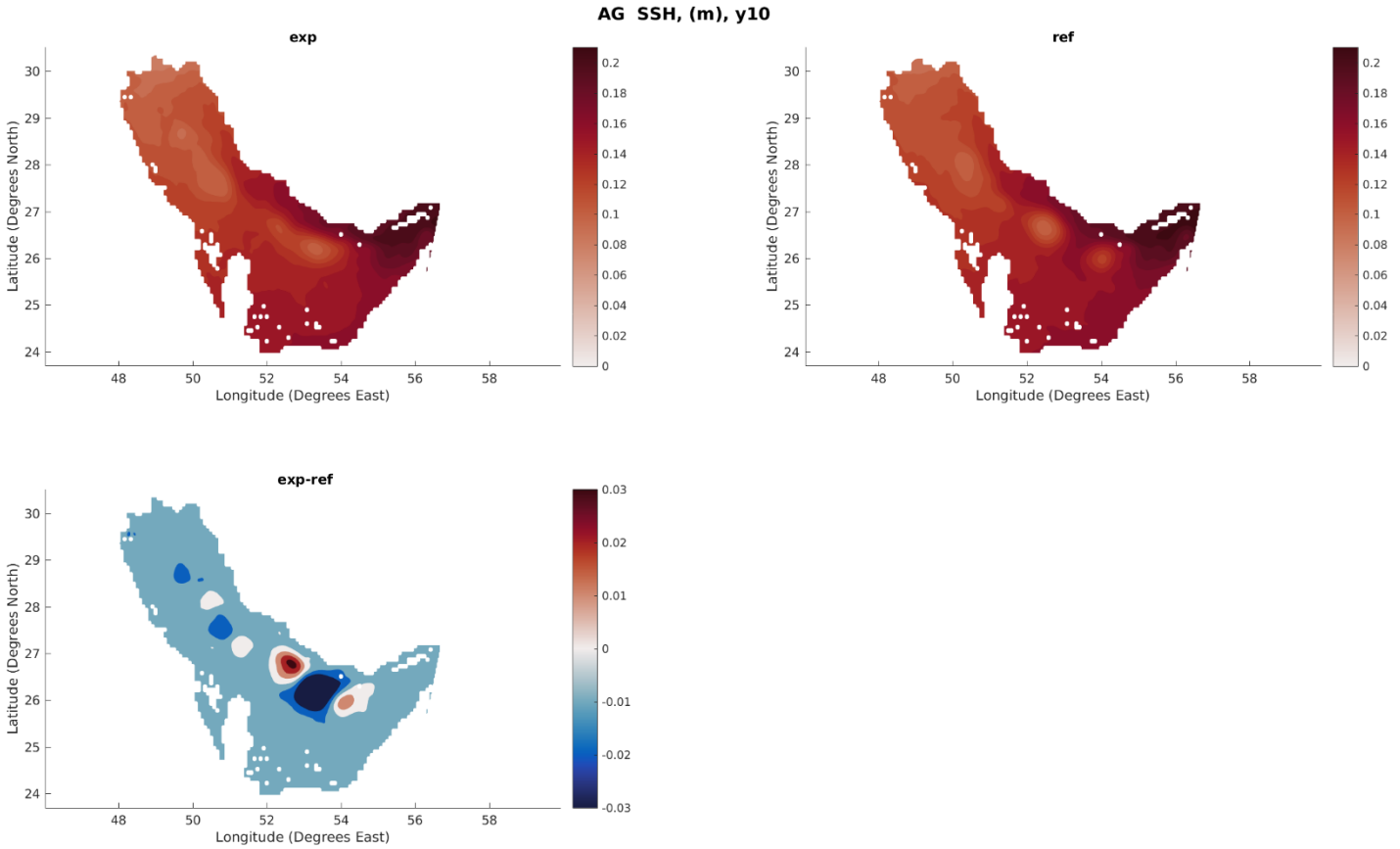

Figure 3-10: Arabian Gulf- Spatial variability of Sea Surface Height average annual values for year 10 of the experiment, the reference and their difference.

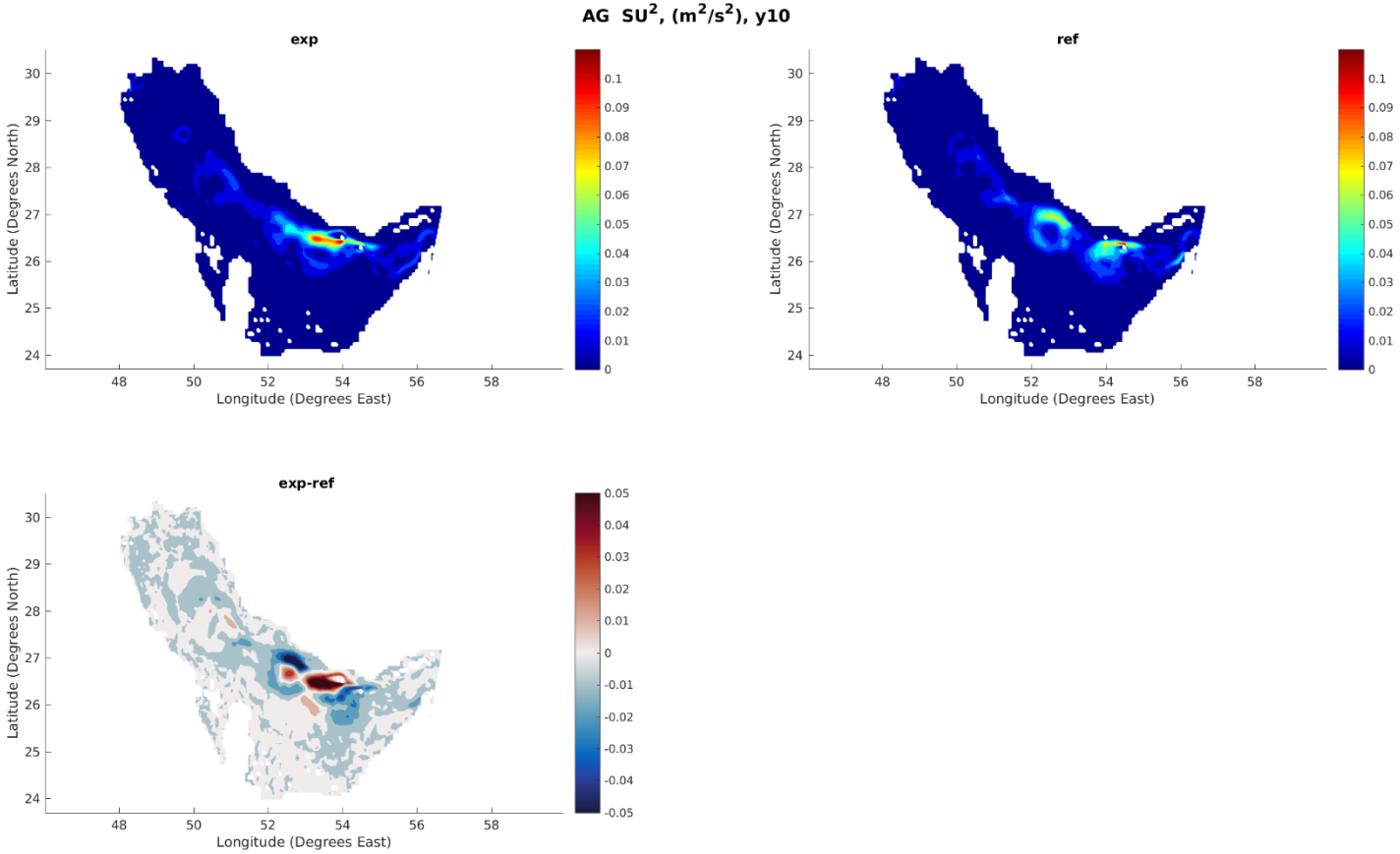

Figure 3-11: Arabian Gulf- Spatial variability of Sea Surface Squared velocity average annual values for year 10 of the experiment, the reference and their difference.

3.2.3 Response of Gulf of Aden

The results for the GoA, denote a decrease in both temperature and salinity, but with surface values manifesting greater variability (Table 3-6).

Additionally, a westward propagation of eddies is observed (Figure 3-15, Figure 3-16) to which the reduced temperature and salinity values may correspond. Possibly, much cooler and less saline water from the AS intrudes further into the gulf, as can be seen on the eastern part of the basin in Figure 3-12 and Figure 3-13, which illustrate the spatial variability of SSS and SST respectively. These eddy features may prevent the horizontal advection of the saline RSOW, therefore the salinity of the gulf is reduced. Moreover, the map of SST (Figure 3-13) indicates that warmer water is restrained closer to the strait, at the western part of the gulf, which may be connected to the eddy features mentioned above.

Observing the maps of SSS and SST (Figure 3-12, Figure 3-13) and keeping in mind that their values are an order of magnitude greater from the total basin values (Table 3-6), it seems that the upwelling off the coasts is stronger and possibly seasonal- on the northern coast during summer and on the southern during winter (Table 3-6, Figure 3-12, Figure 3-13). This north-to-south displacement of the upwelling is due to the monsoon’s seasonality, with southwestern winds during summertime and northeastern during winter, resulting in the corresponding Ekman transport and related upwelling.

GoA	Experiment	Reference	Difference (Exp-Ref)
Tau (N/m^2)	0.057	0.052	0.005
Qlat (W/m^2)	115.100	117.565	-2.470
SU^2 (m^2)	0.180	0.140	0.04
T (°C)	13.540	13.629	-0.089
SST (°C)	27.438	27.627	-0.189
S	35.674	35.718	-0.044
SSS	36.302	36.432	-0.130
SSH (m)	0.1883	0.1879	0.0004
Sζ (s^{-1})	3.090e-09	8.86e-08	-8.55e-08

Table 3-6: Gulf of Aden- Average annual values of the results of the experiment and the reference, and their difference.

Furthermore, latent heat flux has decreased (Table 3-6, Figure 3-14) meaning lower evaporation rate, while the kinetic energy has increased (Table 3-6, Figure 3-16) and surface vorticity drops indicating weakened cyclonic circulation.

In conclusion, it seems that the gulf's circulation is dominated by wind forcing, rather than density driven currents.

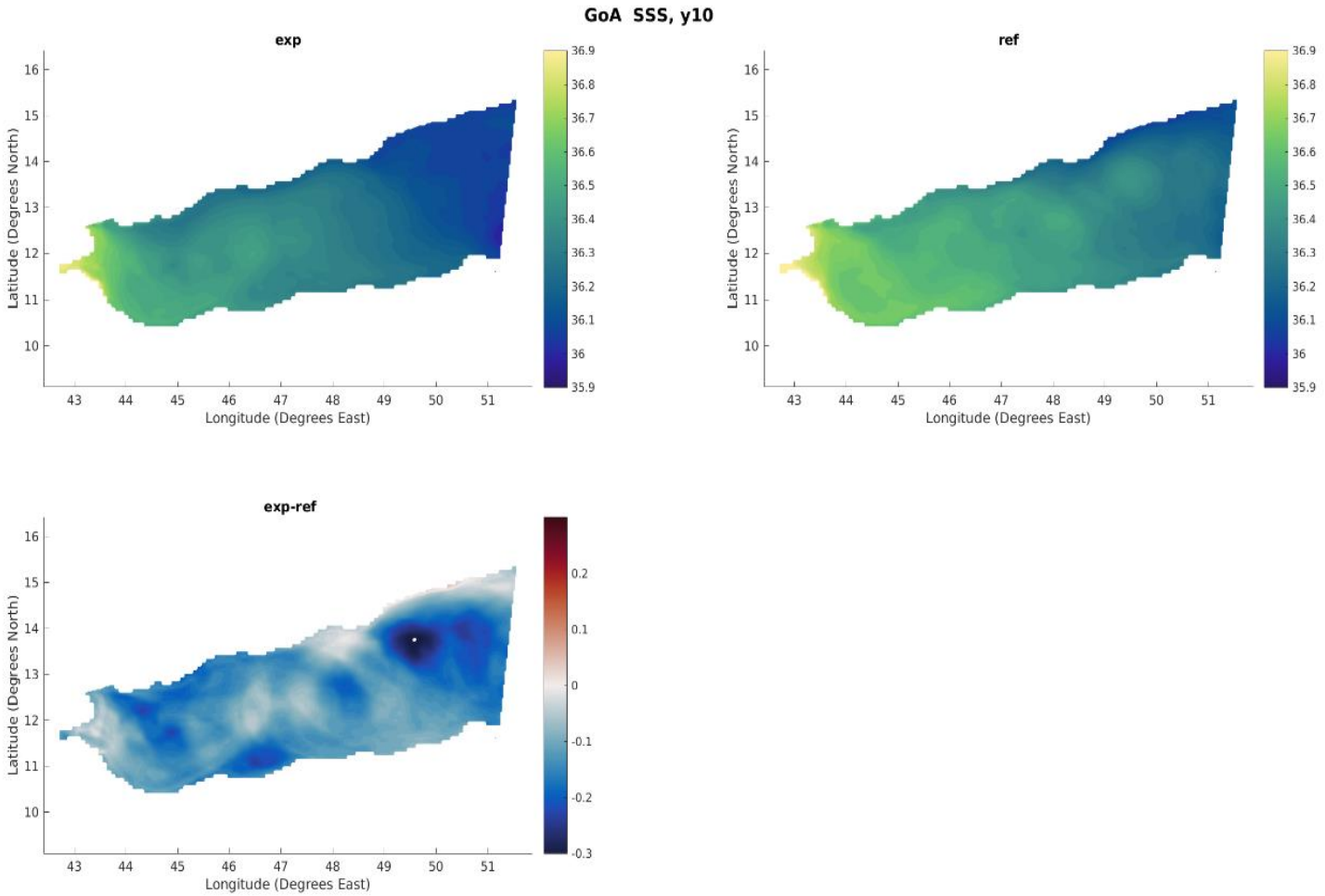

Figure 3-12: Gulf of Aden- Spatial variability of Sea Surface Salinity average annual values for year 10 of the experiment, the reference and their difference.

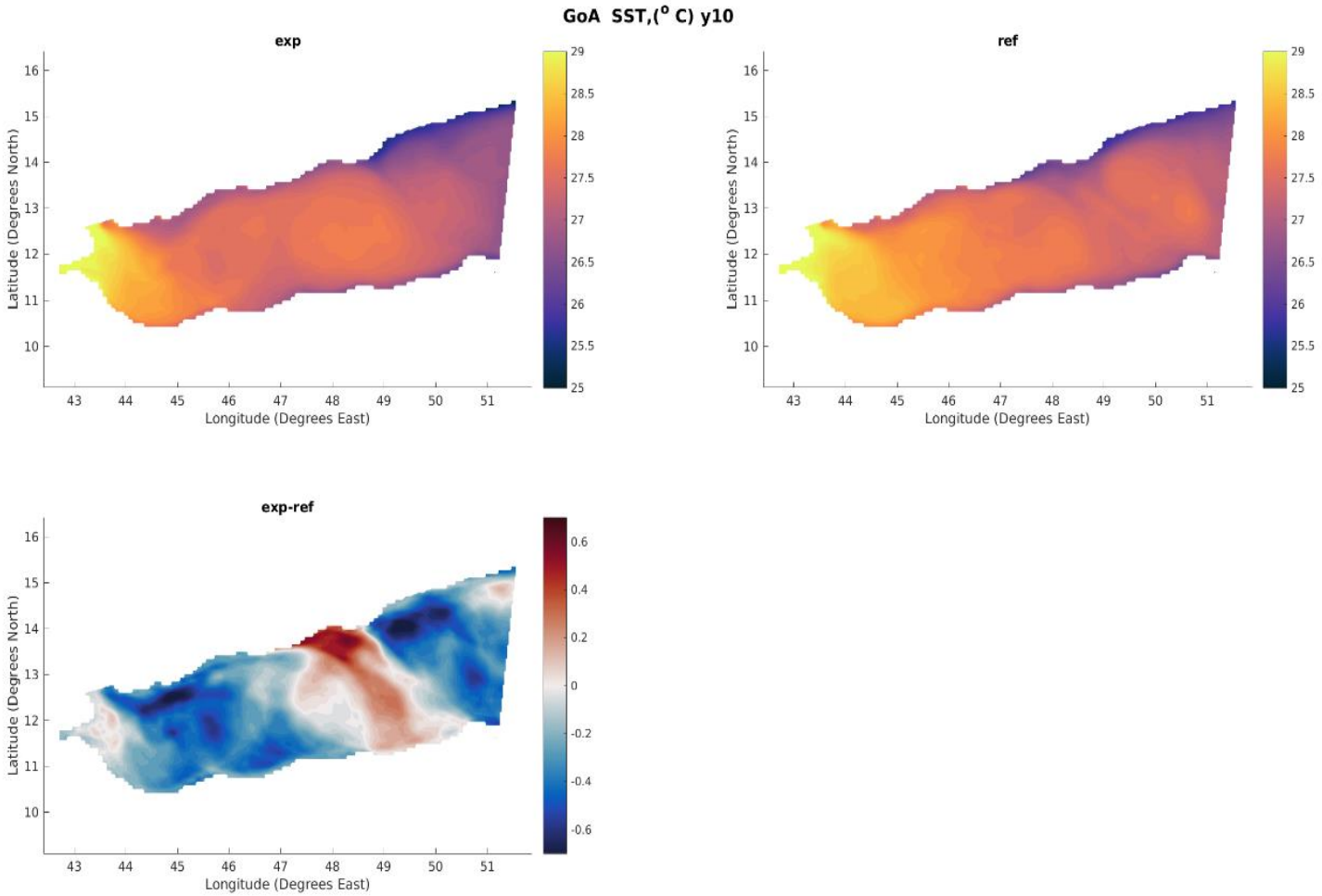

Figure 3-13: Gulf of Aden - Spatial variability of Sea Surface Temperature average annual values for year 10 of the experiment, the reference and their difference.

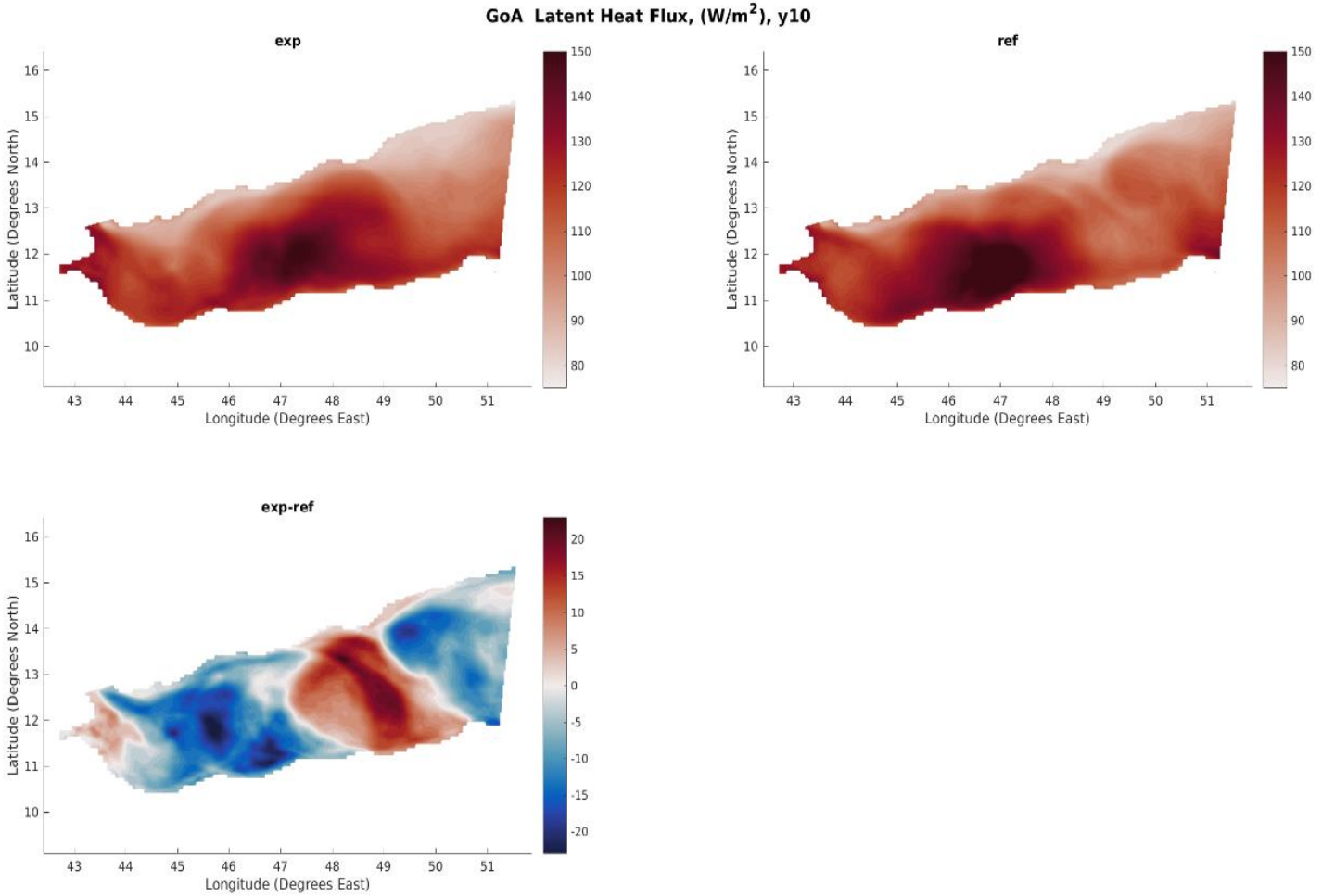

Figure 3-14: Gulf of Aden- Spatial variability of average annual Latent Heat Flux for year 10 of the experiment, the reference and their difference.

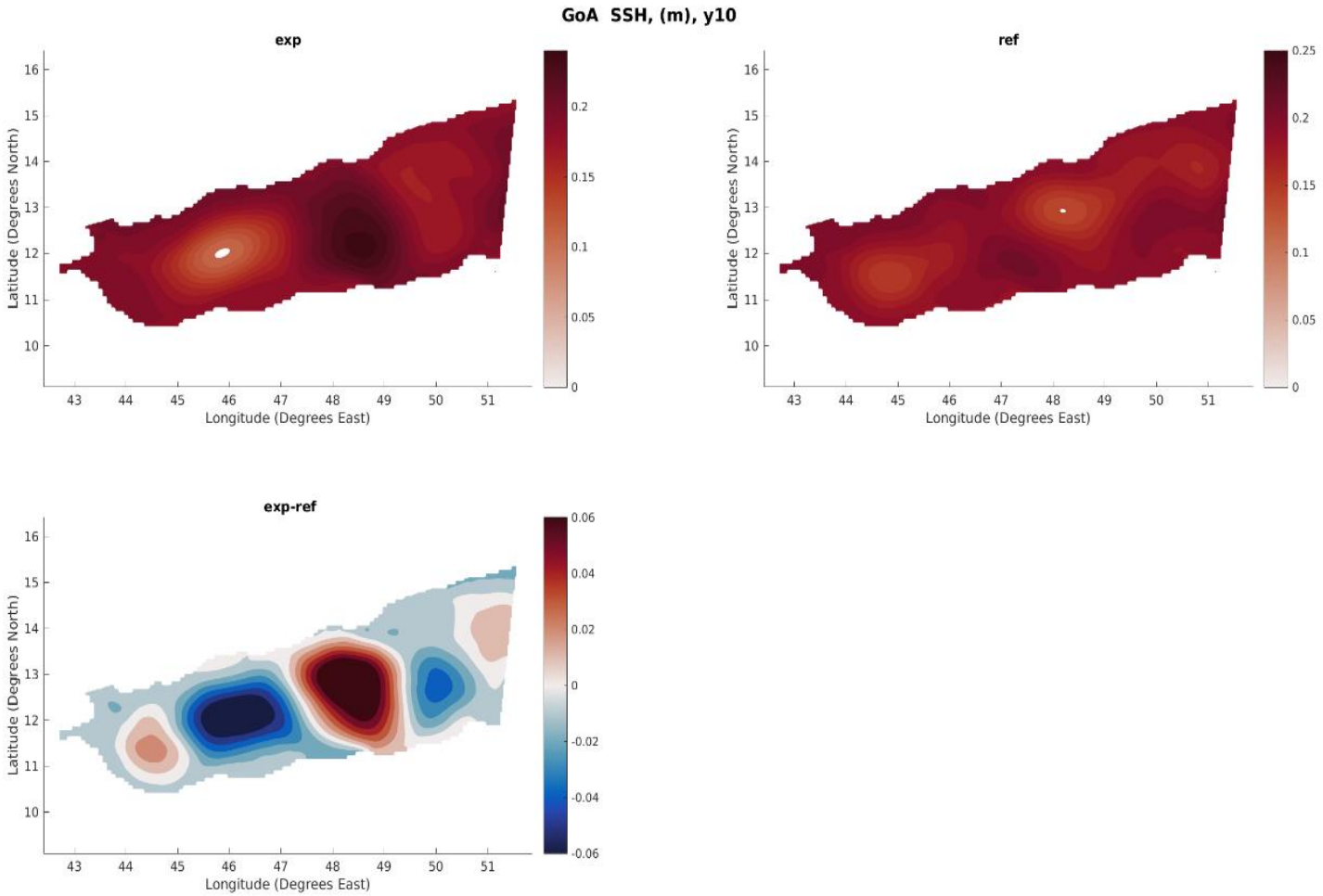

Figure 3-15: Gulf of Aden - Spatial variability of Sea Surface Height average annual values for year 10 of the experiment, the reference and their difference.

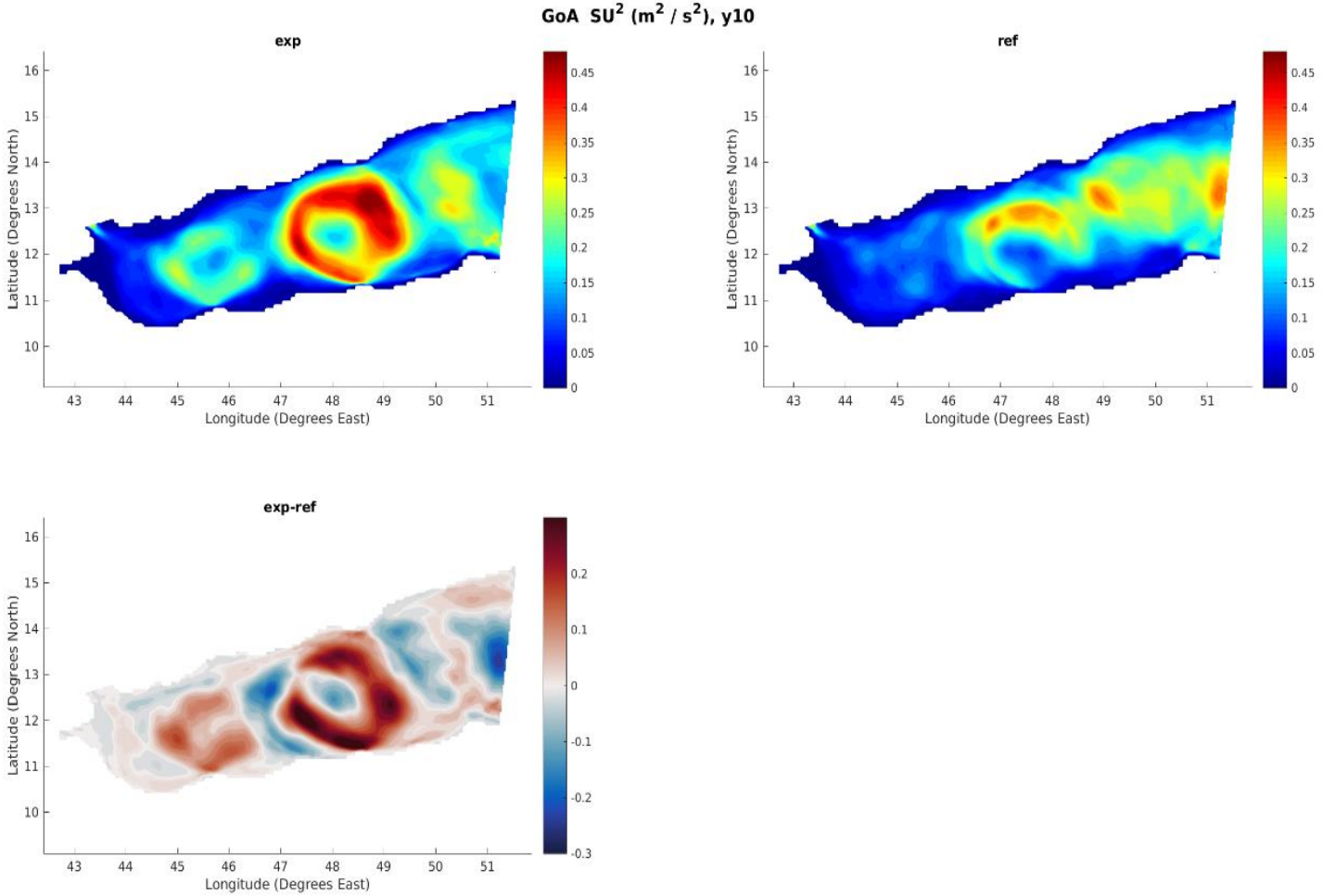

Figure 3-16: Gulf of Aden - Spatial variability of Sea Surface Squared Velocity average annual values for year 10 of the experiment, the reference and their difference.

3.2.4 Response of Gulf of Oman

Compared to GoA, GOM demonstrates similar variability behaviour, with temperature and salinity values dropping.

It appears that the upwelling region off the coast that surrounds the gulf, is extended, while the warmer water of AG does not propagate that far to the east (Figure 3-17, Figure 3-18). The smaller SSS change (Table 3-6), with respect to GoA results, is probably due to weaker upwelling response in this region. Once again, like GoA, surface kinetic energy has increased and eddy features seem to propagate to the east (Figure 3-20, Figure 3-21) while latent heat flux is reduced (Table 3-7, Figure 3-19), indicating wind forcing domination. Furthermore, it appears that the circulation turns from anticyclonic to cyclonic (Table 3-7).

GOM	Experiment	Reference	Difference (Exp-Ref)
Tau (N/m^2)	0.015	0.014	0.001
Qlat (W/m^2)	92.860	95.130	-2.270
SU^2 (m^2s^{-2})	0.040	0.300	0.010
T (°C)	15.490	15.560	-0.070
SST (°C)	28.060	28.240	-0.180
S	35.960	35.980	-0.020
SSS	37.010	37.040	-0.030
SSH (m)	0.172	0.192	-0.020
Sζ (s^{-1})	2.85e-07	-2.85e-07	5.70e-07

Table 3-7: Gulf of Oman- Average annual values of the results of the experiment and the reference, and their difference.

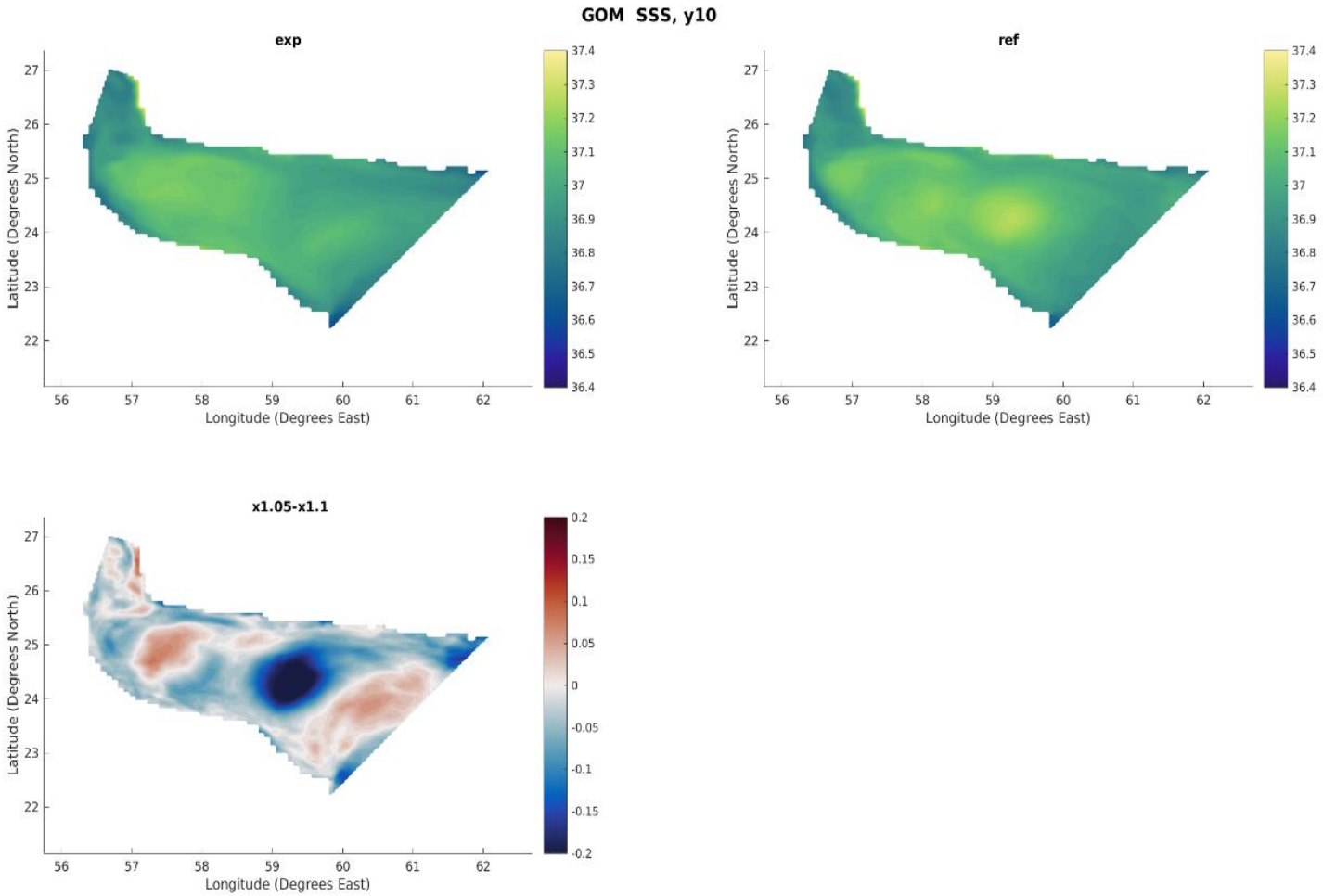

Figure 3-17: Gulf of Oman- Spatial variability of Sea Surface Salinity average annual values for year 10 of the experiment, the reference and their difference.

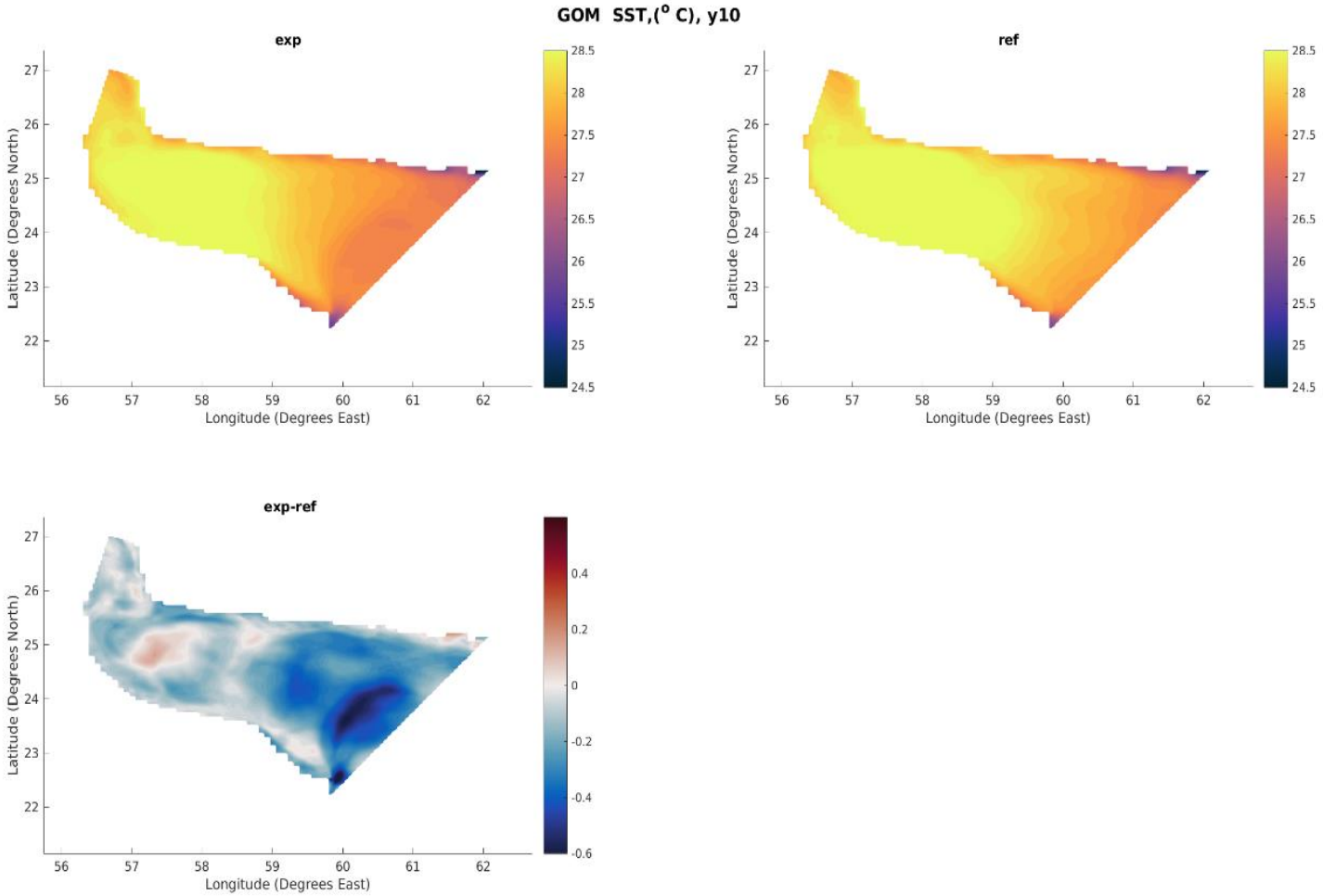

Figure 3-18: Gulf of Oman- Spatial variability of Sea Surface Temperature average annual values for year 10 of the experiment, the reference and their difference.

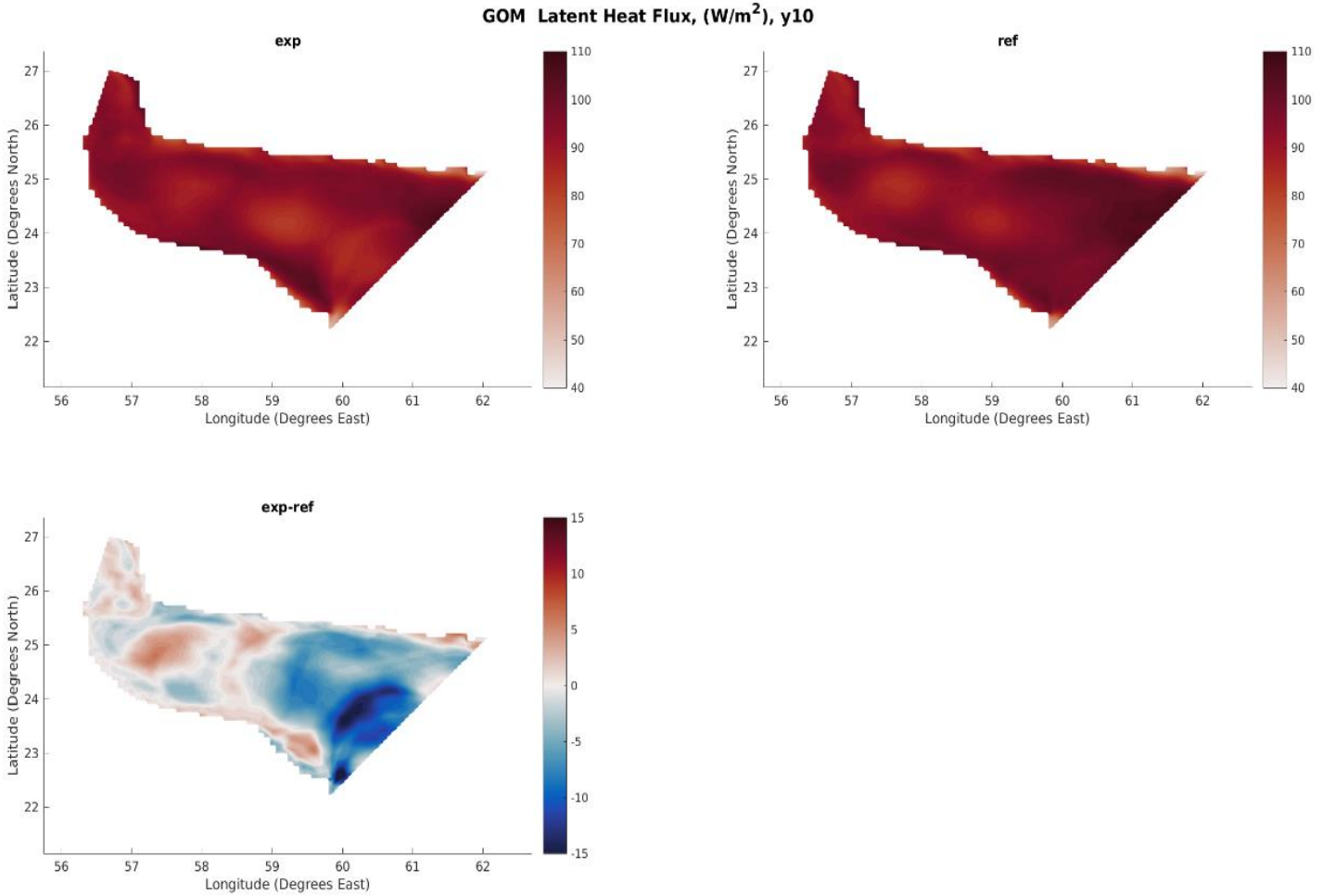

Figure 3-19: Gulf of Oman- Spatial variability of average annual Latent Heat Flux for year 10 of the experiment, the reference and their difference.

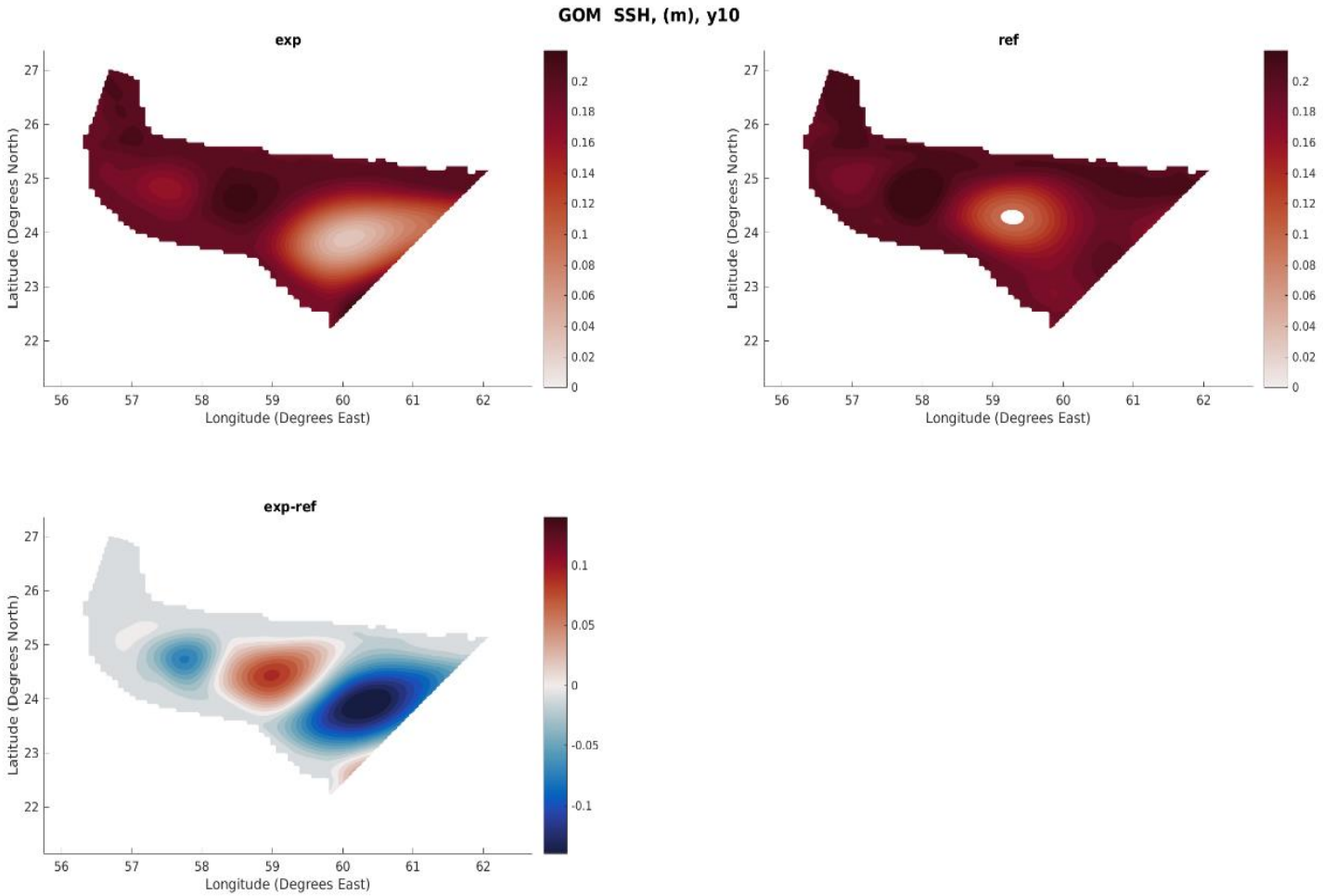

Figure 3-20: Gulf of Oman- Spatial variability of Sea Surface Height average annual values for year 10 of the experiment, the reference and their difference.

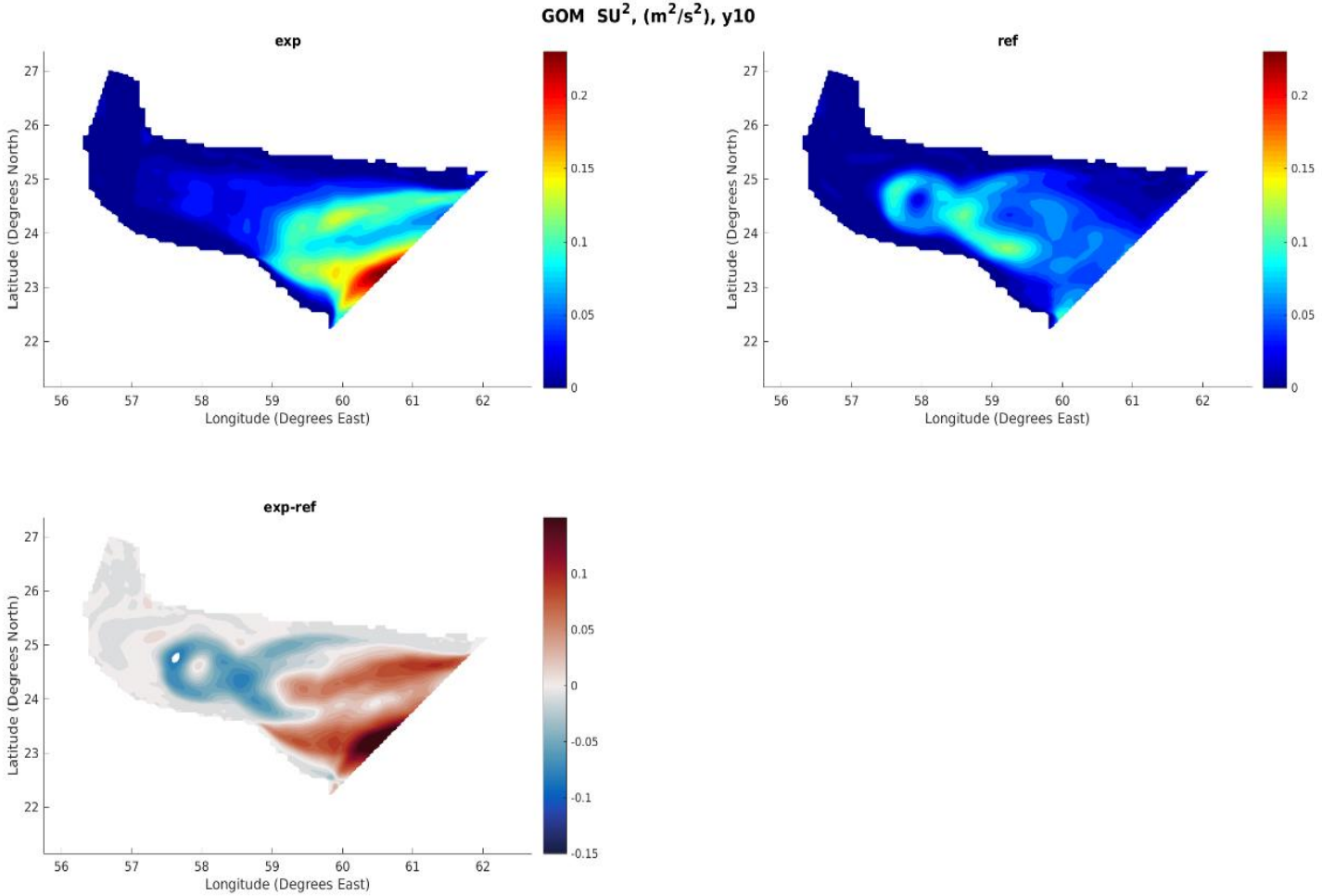

Figure 3-21: Gulf of Oman- Spatial variability of Sea Surface Squared Velocity average annual values for year 10 of the experiment, the reference and their difference.

3.2.5 Response of Arabian Sea

Contrary to the other basins, in AS, temperature has increased by a scale of $O(10^{-3})$, while salinity and surface values decrease (Table 3-8). Also, it appears that latent heat flux has increased, so the evaporation rate is higher (Figure 3-24). The vorticity of the basin is more negative, so surface circulation is more anticyclonic which could lead to enhanced convergence and the corresponding downwelling.

Thus, the increased temperature may indicate that advection of heat by mean circulation, dominates air-sea heat fluxes that are cooling the upper ocean. However, the values regarding the surface of the ocean- especially SST (Table 3-8)- indicate that the enhanced upwelling and the advection of this water even further into the centre of the basin, as seen in Figure 3-23, dominate non-Ekman heat transport. Moreover, it appears that the western boundary current, and hence the Great Whirl, is strengthened, as Figure 3-26 and Figure 3-25 demonstrate through sea surface height and squared velocity fields.

AS	Experiment	Reference	Difference (Exp-Ref)
Tau (N/m^2)	0.092	0.082	0.010
Qlat(W/m^2)	137.7795	136.8230	0.957
SU^2 (m^2s^{-2})	0.1156	0.1044	0.018
T (°C)	7.541	7.536	0.005
SST (°C)	27.140	27.240	-0.100
S	35.145	35.150	-0.005
SSS	36.150	36.168	-0.018
SSH (m)	0.3011	0.3026	-0.0015
Sζ (s^{-1})	-1.16e-07	-0.94e-07	-2.260e-08

Table 3-8: Arabian Sea- Average annual values of the results of the experiment and the reference, and their difference.

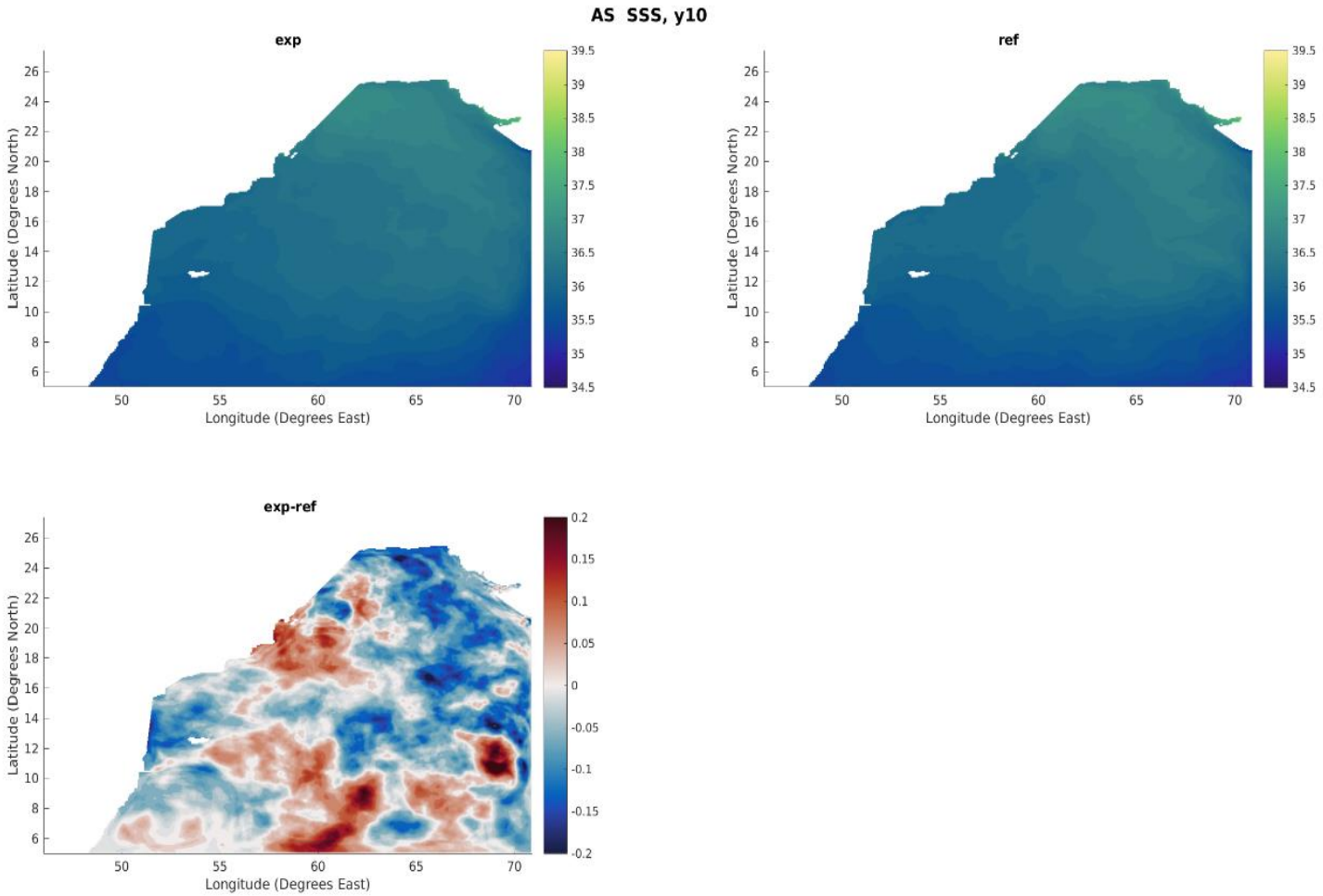

Figure 3-22: Arabian Sea- Spatial variability of Sea Surface Salinity average annual values for year 10 of the experiment, the reference and their difference.

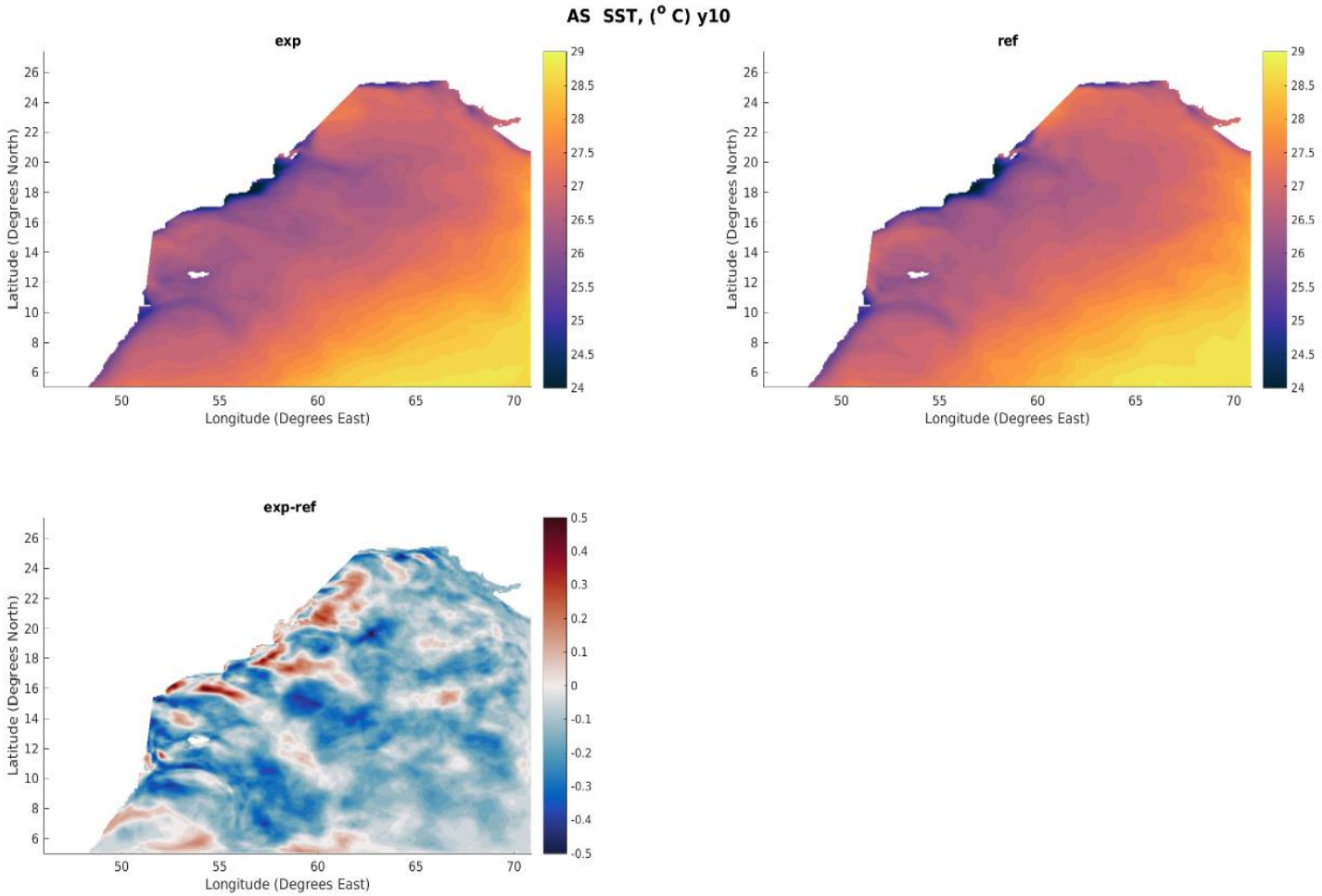

Figure 3-23: Arabian Sea- Spatial variability of Sea Surface Temperature average annual values for year 10 of the experiment, the reference and their difference.

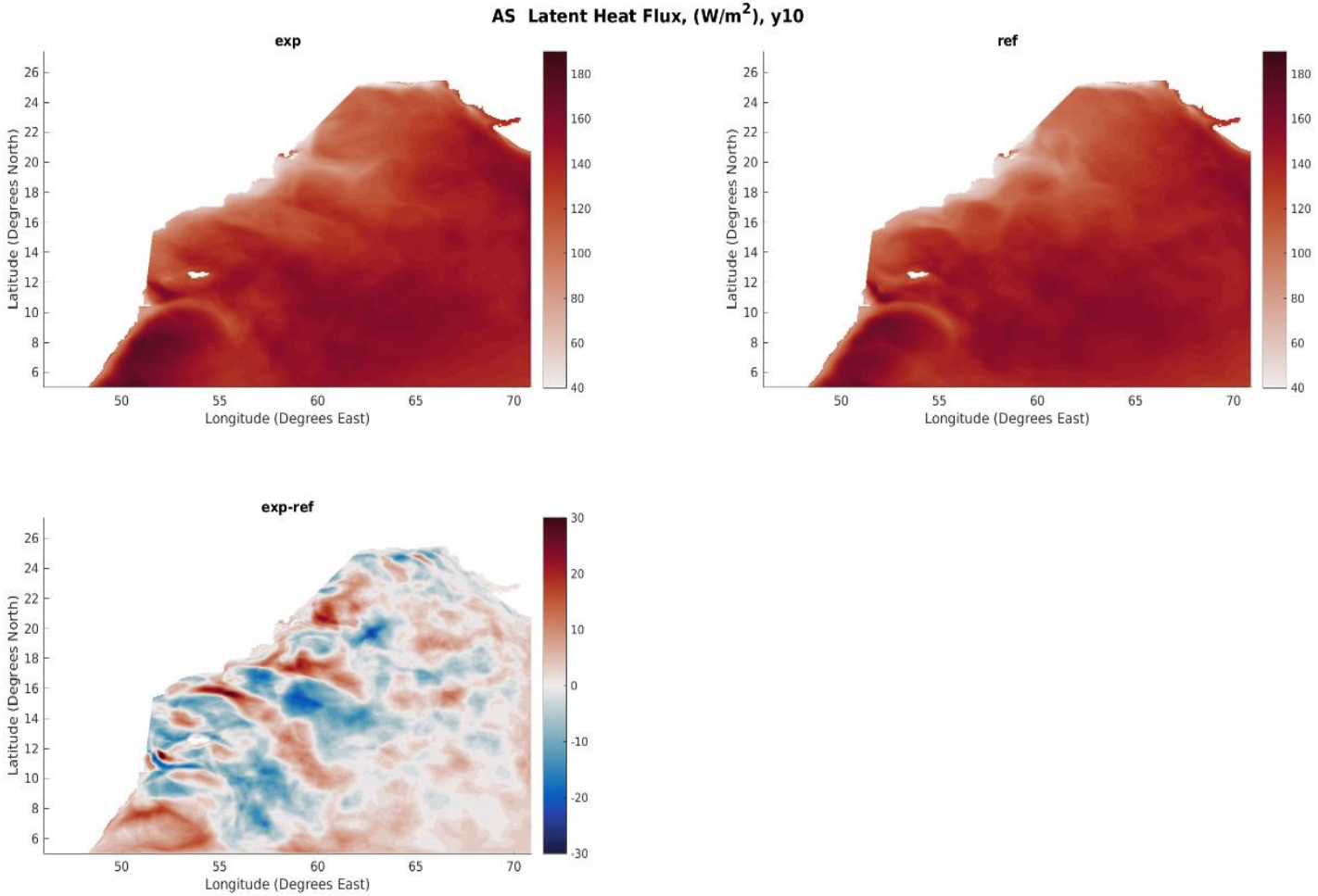

Figure 3-24: Arabian Sea- Spatial variability of average annual Latent Heat Flux for year 10 of the experiment, the reference and their difference.

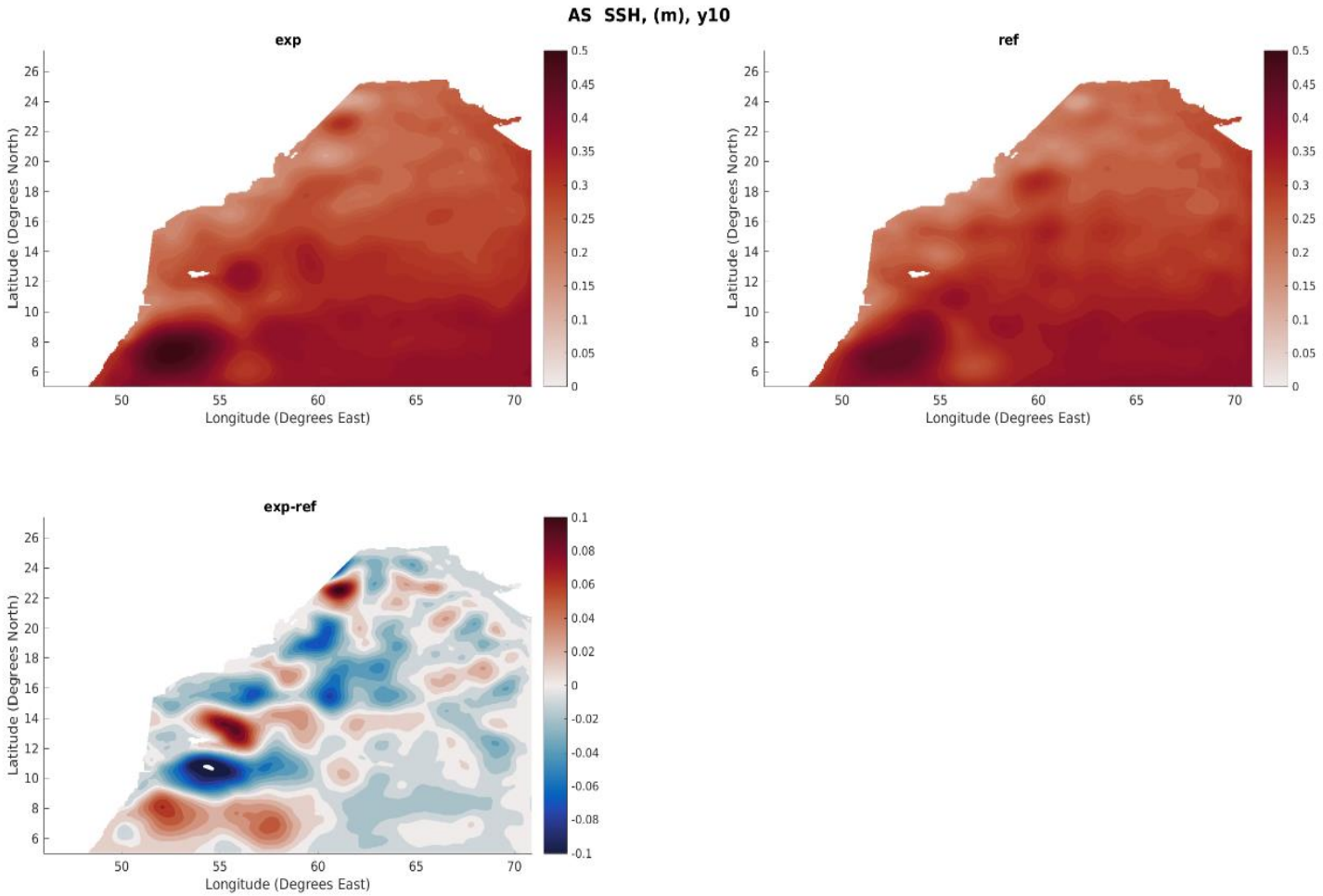

Figure 3-25: Arabian Sea- Spatial variability of Sea Surface Height average annual values for year 10 of the experiment, the reference and their difference.

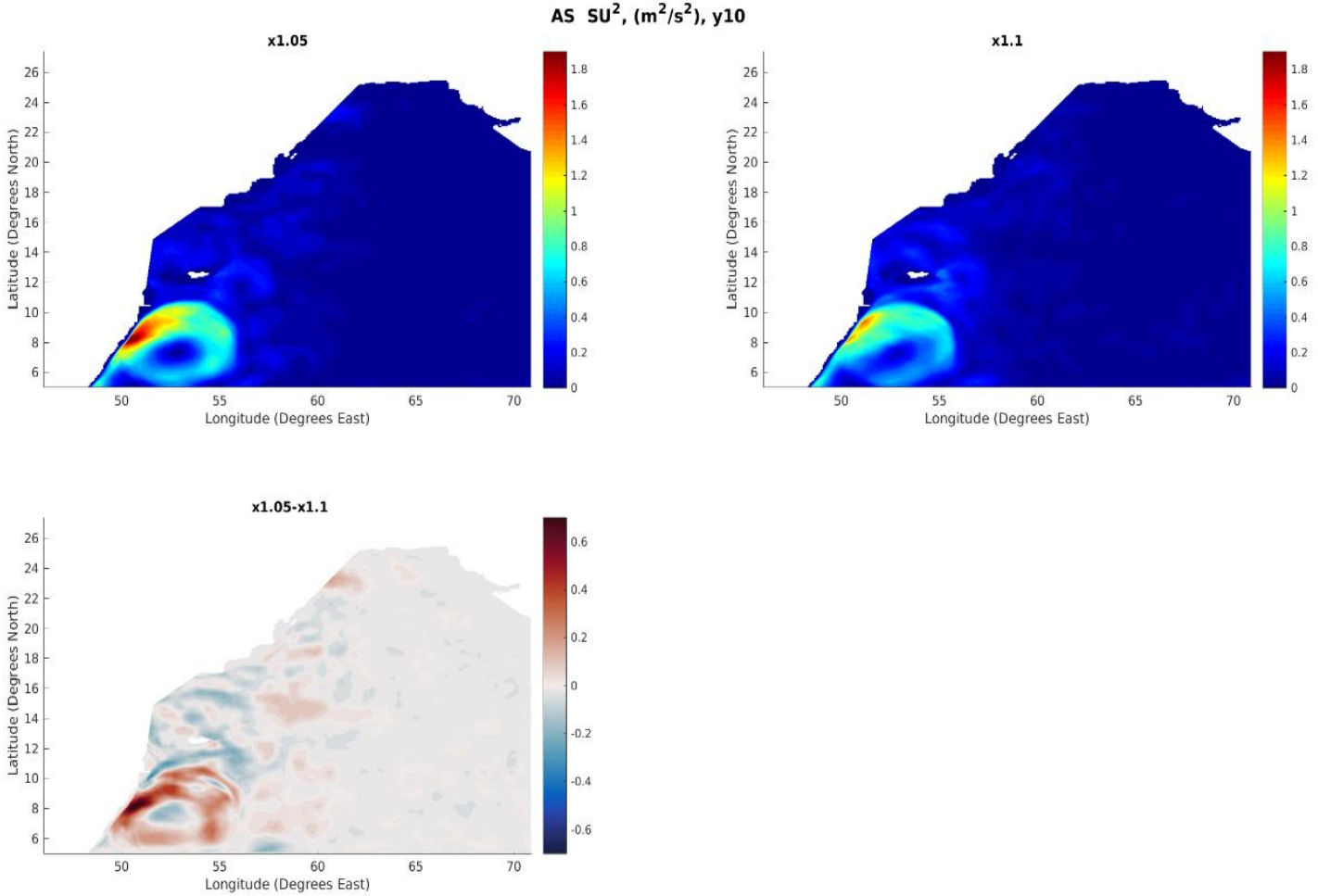

Figure 3-26: Arabian Sea- Spatial variability of Sea Surface Squared Velocity average annual values for year 10 of the experiment, the reference and their difference.

4. Conclusion

In this thesis, we examined the general response of the domain consisting of the Red Sea, the Arabian Gulf, the Gulf of Aden, the Gulf of Oman and the Arabian Sea, at the change of wind strength. This region constitutes a great study area for the assessment of its behavior due to atmospheric forcing, as it includes semi enclosed basins (Red Sea, Arabian Gulf), gulfs that are connected to the ocean directly (Gulf of Aden, Gulf of Oman) and open ocean (Arabian Sea). An experiment was conducted, where the wind speed was increased by a factor of 1.05. Therefore, a comparison was made between main features of the experiment and the reference. We examined their differences, focusing on the annual average values of temperature, salinity and their surface values, sea surface height, latent heat flux and surface kinetic energy. Main objective was to take a closer look on the different response of each basin to the change of wind speed, with respect to the driving forces that regulate their circulation. It appears that the Arabian gulf and the Red Sea share the same mechanisms, that indicate that buoyancy losses associated with the change of wind stress, play a more significant role in the regulation of the flow in these basins and this can be seen in intensification of the volume exchange at the strait. This comes in agreement with bibliography considering enclosed evaporative basins (Geyer and MacCready, 2014; MacCready *et al.*, 2018). On the other hand, Ekman transport reflects the response of the other basins to wind forcing, as the upwelling is enhanced, and their surface mean kinetic energy has increased. The only difference appears on Arabian Sea, where the temperature of the total basin is increasing, probably meaning that advection dominates air-sea fluxes.

Future work could focus on the seasonal variability of this response, as the monsoonal system demonstrates great seasonality and its influence on the region throughout the year

varies. Furthermore, an in-depth investigation of the mesoscale variability of the region could be conducted, as mixing could play an important role in circulation and distribution of features.

5. References

1. Beal, L. M., Ffield, A. and Gordon, A. L. (2000) 'Spreading of Red Sea overflow waters in the Indian Ocean', *Journal of Geophysical Research: Oceans*. John Wiley & Sons, Ltd, 105(C4), pp. 8549–8564. doi: 10.1029/1999JC900306.
2. Bower, A. S. *et al.* (2002) 'Gulf of Aden eddies and their impact on Red Sea Water', *Geophysical Research Letters*. John Wiley & Sons, Ltd, 29(21), p. 2025. doi: 10.1029/2002GL015342.
3. Bower, A. S., Hunt, H. D. and Price, J. F. (2000) 'Character and dynamics of the Red Sea and Persian Gulf outflows', *Journal of Geophysical Research: Oceans*. John Wiley & Sons, Ltd, 105(C3), pp. 6387–6414. doi: 10.1029/1999JC900297.
4. Carton, X., L'hegaret, P. and Baraille, R. (2012) 'Mesoscale variability of water masses in the Arabian Sea as revealed by ARGO floats', *Ocean Sci*, 8, pp. 227–248. doi: 10.5194/os-8-227-2012.
5. Centurioni, L. R. *et al.* (2017) 'Northern Arabian Sea Circulation-Autonomous Research (NASCar): COPYRIGHT This article has been published in Oceanography'. The Oceanography Society, 30(2). doi: 10.5670/oceanog.2017.224.
6. Cessi, P. *et al.* (2014) 'Energetics of Semienclosed Basins with Two-Layer Flows at the Strait', *Journal of Physical Oceanography*, 44(3), pp. 967–979. doi: 10.1175/JPO-D-13-0129.1.
7. Düing, W. *et al.* (1980) 'Arabian Sea Cooling: A Preliminary Heat Budget', *Journal of Physical Oceanography*, 10(2), pp. 307–312. doi: 10.1175/1520-0485(1980)010<0307:ASCAPH>2.0.CO;2.
8. Dussin Raphael, Barnier Bernard, Brodeau Laurent, M. J. M. (2016) *The Making Of the DRAKKAR FORCING SET DFS5*. Grenoble, France. Available at: https://www.drakkar-ocean.eu/publications/reports/report_DFS5v3_April2016.pdf#page=1&zoom=auto,-256,848.
9. Fischer, A. S. *et al.* (2002) 'Mesoscale eddies, coastal upwelling, and the upper-ocean heat budget in the Arabian Sea', *Deep Sea Research Part II: Topical Studies in Oceanography*. Pergamon, 49(12), pp. 2231–2264. doi: 10.1016/S0967-0645(02)00036-X.
10. Geyer, W. R. and MacCready, P. (2014) 'The Estuarine Circulation', *Annual Review of Fluid Mechanics*. Annual Reviews , 46(1), pp. 175–197. doi: 10.1146/annurev-fluid-010313-141302.

11. Johns, W. E. *et al.* (2003) ‘Observations of seasonal exchange through the Straits of Hormuz and the inferred heat and freshwater budgets of the Persian Gulf’, *Journal of Geophysical Research*. John Wiley & Sons, Ltd, 108(C12), p. 3391. doi: 10.1029/2003JC001881.

12. Langodan, S. *et al.* (2016) ‘A high-resolution assessment of wind and wave energy potentials in the Red Sea’, *Applied Energy*. Elsevier, 181, pp. 244–255. doi: 10.1016/J.APENERGY.2016.08.076.

13. Lee, C. M. *et al.* (2000) ‘The upper-ocean response to monsoonal forcing in the Arabian Sea: seasonal and spatial variability’, *Deep Sea Research Part II: Topical Studies in Oceanography*. Pergamon, 47(7–8), pp. 1177–1226. doi: 10.1016/S0967-0645(99)00141-1.

14. Li, G. *et al.* (2011) ‘Revisiting the trend of the tropical and subtropical Pacific surface latent heat flux during 1977–2006’, *Journal of Geophysical Research*. John Wiley & Sons, Ltd, 116(D10), p. D10115. doi: 10.1029/2010JD015444.

15. MacCready, P. *et al.* (2018) ‘Estuarine Exchange Flow Is Related to Mixing through the Salinity Variance Budget’, *Journal of Physical Oceanography*, 48(6), pp. 1375–1384. doi: 10.1175/JPO-D-17-0266.1.

16. Madec, G. *et al.* (1998) ‘OPA 8.1 Ocean General Circulation Model Reference Manual’, *Notes du Pôle de Modélisation, Institut Pierre Simon Laplace*, (11), p. 97pp. Available at: https://www.nemo-ocean.eu/wp-content/uploads/Doc_OPA8.1.pdf.

17. Madec, G. (2016) *NEMO ocean engine*. Available at: https://www.nemo-ocean.eu/wp-content/uploads/NEMO_book.pdf.

18. Michael Reynolds, R. (1993) ‘Physical oceanography of the Gulf, Strait of Hormuz, and the Gulf of Oman—Results from the Mt Mitchell expedition’, *Marine Pollution Bulletin*. Pergamon, 27, pp. 35–59. doi: 10.1016/0025-326X(93)90007-7.

19. Morcos, S. A. and AbdAllah, A. M. (2012) ‘Oceanography of the Gulf of Aden: John Murray–Mabahiss Expedition 1933–1934 Revisited’, *The Egyptian Journal of Aquatic Research*. Elsevier, 38(2), pp. 77–91. doi: 10.1016/J.EJAR.2012.12.001.

20. Murray, S. P. and Johns, W. (1997) ‘Direct observations of seasonal exchange through the Bab el Mandab Strait’, *Geophysical Research Letters*. John Wiley & Sons, Ltd, 24(21), pp. 2557–2560. doi: 10.1029/97GL02741.

21. Patzert, W. C. (1974) ‘Wind-induced reversal in Red Sea circulation’, *Deep Sea Research and Oceanographic Abstracts*. Elsevier, 21(2), pp. 109–121. doi: 10.1016/0011-7471(74)90068-0.

22. Pous, S., Carton, X. and Lazure, P. (2013) ‘A Process Study of the Wind-Induced Circulation in the Persian Gulf’, *Open Journal of Marine Science*. Scientific Research Publishing, Inc, 03(01), pp. 1–11. doi: 10.4236/ojms.2013.31001.

23. Pous, S. P., Carton, X. and Lazure, P. (2004) ‘Hydrology and circulation in the Strait of Hormuz and the Gulf of Oman—Results from the GOGP99 Experiment: 2. Gulf of Oman’, *Journal of Geophysical Research*. John Wiley & Sons, Ltd, 109(C12), p. C12038. doi: 10.1029/2003JC002146.

24. Rezaei-Latifi, A. and Hosseinibalam, F. (2015) ‘An estimate of the surface heat fluxes transfer of the Persian Gulf with the overlying atmosphere’, *Journal of Radiation Research and Applied Sciences*. No longer published by Elsevier, 8(3), pp. 354–361. doi: 10.1016/J.JRRAS.2015.02.002.

25. Roberts C.D. *et al.* (2017) ‘Surface flux and ocean heat transport convergence contributions to seasonal and interannual variations of ocean heat content’, *Journal of Geophysical Research: Oceans.* John Wiley & Sons, Ltd, 122(1), pp. 726-744. doi: 10.1002/2016JC012278.

26. Schott, F. *et al.* (1982) ‘Variability of the Somali Current System during the Onset of the Southwest Monsoon, 1979’, *Journal of Physical Oceanography*, 12(12), pp. 1343–1357. doi: 10.1175/1520-0485(1982)012<1343:VOTSCS>2.0.CO;2.

27. Schott, F. (1983) ‘Monsoon response of the Somali Current and associated upwelling’, *Progress in Oceanography*. Pergamon, 12(3), pp. 357–381. doi: 10.1016/0079-6611(83)90014-9.

28. Schott, F. *et al.* (1997) ‘Summer monsoon response of the Northern Somali Current, 1995’, *Geophysical Research Letters*. John Wiley & Sons, Ltd, 24(21), pp. 2565–2568. doi: 10.1029/97GL00888.

29. Schott, F. A. and Fischer, J. (2000) ‘Winter monsoon circulation of the northern Arabian Sea and Somali Current’, *Journal of Geophysical Research: Oceans*. John Wiley & Sons, Ltd, 105(C3), pp. 6359–6376. doi: 10.1029/1999JC900312.

30. Schott, F. A., Xie, S.-P. and McCreary, J. P. (2009) ‘Indian Ocean circulation and climate variability’, *Reviews of Geophysics*. John Wiley & Sons, Ltd, 47(1), p. RG1002. doi: 10.1029/2007RG000245.

31. Sofianos, S. and Johns, W. E. (2015) ‘Water Mass Formation, Overturning Circulation, and the Exchange of the Red Sea with the Adjacent Basins’, in. Springer, Berlin, Heidelberg, pp. 343–353. doi: 10.1007/978-3-662-45201-1_20.

32. Sofianos, S. S. and Johns, W. E. (2002) 'An Oceanic General Circulation Model (OGCM) investigation of the Red Sea circulation, 1. Exchange between the Red Sea and the Indian Ocean', *Journal of Geophysical Research*. John Wiley & Sons, Ltd, 107(C11), p. 3196. doi: 10.1029/2001JC001184.

33. Sofianos, S. S. and Johns, W. E. (2007) 'Observations of the summer Red Sea circulation', *Journal of Geophysical Research*. John Wiley & Sons, Ltd, 112(C6), p. C06025. doi: 10.1029/2006JC003886.

34. Sofianos, S. S., Johns, W. E. and Murray, S. P. (2002) 'Heat and freshwater budgets in the Red Sea from direct observations at Bab el Mandeb', *Deep Sea Research Part II: Topical Studies in Oceanography*. Pergamon, 49(7–8), pp. 1323–1340. doi: 10.1016/S0967-0645(01)00164-3.

35. Sultan, S. A. R. and Ahmad, F. (1993) 'Surface and oceanic heat fluxes in the Gulf of Oman', *Continental Shelf Research*. Pergamon, 13(10), pp. 1103–1110. doi: 10.1016/0278-4343(93)90043-W.

36. Sultan, S. and Ahmad, F. (1997) *Heat budget of the Gulf of Aden: surface, advective and upwelling heat fluxes.*, *Oceanologica Acta*, Éditions scientifiques et médicales Elsevier SAS, 20(5), pp. 665-672.

37. Swift, S. A. and Bower, A. S. (2003) 'Formation and circulation of dense water in the Persian/Arabian Gulf', *Journal of Geophysical Research*. John Wiley & Sons, Ltd, 108(C1), p. 3004. doi: 10.1029/2002JC001360.

38. Vecchi, G. A. *et al.* (2004) 'Ocean–Atmosphere Covariability in the Western Arabian Sea*', *Journal of Climate*, 17(6), pp. 1213–1224. doi: 10.1175/1520-0442(2004)017<1213:OCITWA>2.0.CO;2.

39. Wang, B. *et al.* (1999) 'Choice of South Asian Summer Monsoon Indices', *Bulletin of the American Meteorological Society*, American Meteorological Society, 80(4), pp.629-638. doi: 10.1175/1520-0477(1999)080<0629:COSASM>2.0.CO;2.

40. Wang, H. *et al.* (2018) 'Seasonal Cycle and Annual Reversal of the Somali Current in an Eddy-Resolving Global Ocean Model', *Journal of Geophysical Research: Oceans*. John Wiley & Sons, Ltd, 123(9), pp. 6562–6580. doi: 10.1029/2018JC013975.

41. Yao, F. and Johns, W. E. (2010) 'A HYCOM modeling study of the Persian Gulf: 1. Model configurations and surface circulation', *Journal of Geophysical Research*. John Wiley & Sons, Ltd, 115(C11), p. C11017. doi: 10.1029/2009JC005781.